frontiers | Frontiers in Earth Science

TYPE Original Research
PUBLISHED 26 July 2022
DOI 10.3389/feart.2022.826143

OPEN ACCESS

EDITED BY
Steffen Mischke,
University of Iceland, Iceland

REVIEWED BY
Allan Chivas,
University of Wollongong, Australia
Gaolei Jiang,
Lanzhou University, China
Lucy Roberts,
Aarhus University, Denmark

*CORRESPONDENCE
Nicole Börner,
nicole.boerner@tu-braunschweig.de

SPECIALTY SECTION
This article was submitted to Quaternary Science, Geomorphology and Paleoenvironment, a section of the journal Frontiers in Earth Science

RECEIVED 30 November 2021
ACCEPTED 29 June 2022
PUBLISHED 26 July 2022

CITATION
Börner N, Jochum KP, Stuhr M, Abstein M, Plessen B, Frenzel P, Wang J, Zhu L and Schwalb A (2022), Late Quaternary changes in moisture availability and weathering intensity on the central Tibetan Plateau indicated by chemical signatures of ostracod shells. *Front. Earth Sci.* 10:826143. doi: 10.3389/feart.2022.826143

Late Quaternary changes in moisture availability and weathering intensity on the central Tibetan Plateau indicated by chemical signatures of ostracod shells

Nicole Börner[1]*, Klaus Peter Jochum[2], Marleen Stuhr[3,4], Michelle Abstein[1], Birgit Plessen[5], Peter Frenzel[6], Junbo Wang[7], Liping Zhu[7] and Antje Schwalb[1]

[1]Institute of Geosystems and Bioindication, Technische Universität Braunschweig, Braunschweig, Germany, [2]Climate Geochemistry Department, Max Planck Institute for Chemistry, Mainz, Germany, [3]Interuniversity Institute for Marine Sciences in Eilat (IUI), Eilat, Israel, [4]Mina and Everard Goodman Faculty of Life Sciences, Bar-Ilan University (BIU), Ramat Gan, Israel, [5]Helmholtz Centre Potsdam, GFZ German Research Centre for Geosciences, Section Climate Dynamics and Landscape Evolution, Potsdam, Germany, [6]Institut für Geowissenschaften, Friedrich-Schiller-Universität Jena, Jena, Germany, [7]Institute of Tibetan Plateau Research, Chinese Academy of Sciences, Beijing, China

High-resolution multi-proxy records from two lakes on the southern Tibetan Plateau, Nam Co and Tangra Yumco, are used to infer long-term variations in the Asian monsoon system with a novel set of ostracod shell chemistry proxies. We track the moisture evolution since the Last Glacial Maximum using the trace element, rare earth element (REE) and stable isotope composition of ostracod shells. The sediment records covering the past 18.8 cal. ka BP and 17.4 cal. ka BP, respectively, demonstrate the suitability of REEs as indicators of weathering intensity and thus hydrological changes and moisture sources in the catchment. In Nam Co, high concentrations of light REEs between 14 and 13 cal. ka BP suggest an increased drainage from the glaciated Nyainqêngtanglha Mountains in the south, pointing to meltwater input. REEs in ostracod shells therefore provide additional information on water sources critical for the interpretation of stable isotope records. Mg/Ca, Sr/Ca, and Ba/Ca ratios reflect salinity and thus changes in effective moisture. Asynchronous behavior of Mg/Ca, Sr/Ca, and Ba/Ca ratios are controlled by changes in dominance of precipitating carbonate minerals in the lake. Synchronous behavior reflects calcite precipitation, indicating low-Mg/Ca warm-wet conditions. Constantly low Sr/Ca ratios reflect aragonite precipitation, indicating high-Mg dry conditions. Increased Sr/Ca and Ba/Ca relative to Mg/Ca ratios show monohydrocalcite precipitation, indicating high-Mg/Ca cold-dry conditions. Furthermore, Fe/Ca, Mn/Ca and U/Ca ratios in ostracods reflect changes in oxygen saturation in lake bottom waters controlled by lake level and microbial activity. The paleoclimate histories reconstructed from Nam Co and Tangra Yumco show high similarity throughout the late Quaternary. We identified two major dry periods, corresponding to Heinrich 1 and the Younger Dryas, followed by

strengthening in Indian summer monsoon precipitation. The early Holocene is characterized by a moisture maximum, reflecting abundant water supply by a strong ISM. A time-delayed shift to dry conditions occurred at 2.6 cal. ka BP at Tangra Yumco, and at 2 cal. ka BP at Nam Co, resulting in decreasing lake levels, caused by weakened monsoon intensity due to a southeastward migration of the ISM-Westerly boundary with an estimated velocity of approximately 600 m per year.

KEYWORDS

trace element geochemistry, stable isotopes, Asian monsoon system, rare earth elements (REE), Tibetan Plateau, paleohydrology, carbonate precipitation

1 Introduction

The Tibetan Plateau is one of the most sensitive areas to global climate change. Since 1960, precipitation has risen by 12%, and temperatures have increased by 0.4°C per decade, which is three times the global average (Lin et al., 2017). This has led to glacier retreat and degradation of permafrost (Yao et al., 2012; Cheng and Jin, 2013). Situated in the transition zone between East Asian monsoon (EAM), Indian summer monsoon (ISM) and Westerlies, the high elevation of the Tibetan Plateau affects the global atmospheric circulation (Ye and Wu, 1998) which makes it a key region to study the Asian monsoon system.

Although numerous studies reconstructed Holocene monsoon variability in different regions of the Tibetan Plateau (Zhu et al., 2009; An et al., 2012; He et al., 2018; Thompson et al., 2018), regional variability in timing and magnitude of monsoon precipitation led to contrary conclusions regarding the interaction of different circulation systems within the Asian monsoon system. A synthesis of eleven lake records from arid central Asia concluded, that the patterns of moisture variation are out-of-phase between Westerly-influenced regions and areas influenced by the Asian monsoon (Chen et al., 2008, 2019). Contrasting results were reported in other studies, which indicated more or less in-phase changes during the late Quaternary (Herzschuh, 2006; Wünnemann et al., 2018).

In the present study, we compare high-resolution multi-proxy records from two lakes on the southern Tibetan Plateau, Nam Co and Tangra Yumco, to infer long-term variations in strength and extent of the Asian monsoon system. Nam Co in the eastern part of the southern Tibetan Plateau is clearly influenced by the ISM, whereas Tangra Yumco is located on the transition between Westerlies and ISM (Ahlborn et al., 2016a). In closed basin lakes like Nam Co and Tangra Yumco, lake level changes are an important indicator of changes in water balance. Thus, lacustrine sediments are sensitive archives of environmental changes. Typically, within these sediments calcite shells of ostracods are well preserved microfossils. Ostracods are abundant in Tibetan Plateau lakes and sensitive to environmental conditions (Mischke, 2012; Akita et al., 2016).

The most dominant ostracod taxon in Nam Co and Tangra Yumco is *Leucocytherella sinensis* Huang, 1985, an endemic species widely distributed in high altitude water bodies (above 4,000 m) on the southern, central and western Tibetan Plateau. It inhabits cold and saline aquatic environments with salinities of 0–13‰ (Huang et al., 1985). *Leucocytherella sinensis* is an ecologically opportunistic species possessing a wide ecological tolerance (Wrozyna et al., 2009; Peng et al., 2013) dominating Ca-depleted brackish waters (Akita et al., 2016). The species has a high propagating ability and strong adaptability (Li et al., 2002). Reproduction starts in late spring (May/June) with several subsequent generations until September (Börner et al., 2017).

The geochemical composition (e.g. stable isotopes and trace elements) of their calcite shells provides valuable information about past hydrological changes (Holmes et al., 2007; Mischke et al., 2008, 2010; Zhang et al., 2009). Stable oxygen and carbon isotopes as well as Mg/Ca and Sr/Ca ratios of ostracod shells have been used in many studies to reconstruct temperature and salinity changes (Holmes, 1996; Holmes and De Deckker, 2012). The use of Ba/Ca, Fe/Ca and Mn/Ca ratios is less common and there exists only one study using REEs in ostracod shells (Börner et al., 2013). Nevertheless, from previous studies it became clear that the incorporation of elements into the shell calcite of ostracods is controlled by a variety of factors, which can differ between lakes showing regional variability. Therefore, a modern calibration study was conducted by Börner et al. (2017) to identify those controlling factors in lakes from the southern Tibetan Plateau, including Nam Co and Tangra Yumco. For further details see Supplementary Material.

Using ostracod shell chemistry records we 1) test the suitability of REEs and trace elements in ostracod shells to reconstruct environmental changes in Lake Nam Co, where a detailed climate history since the LGM is already available (Zhu et al., 2008; Daut et al., 2010; Günther et al., 2015; Kasper et al., 2015), 2) compare REE, trace element and stable isotope inferred changes, and 3) assess the interaction of the ISM and Westerlies based on a comparison of the Nam Co and Tangra Yumco records to identify synchronous and asynchronous climatic changes along this east-west transect.

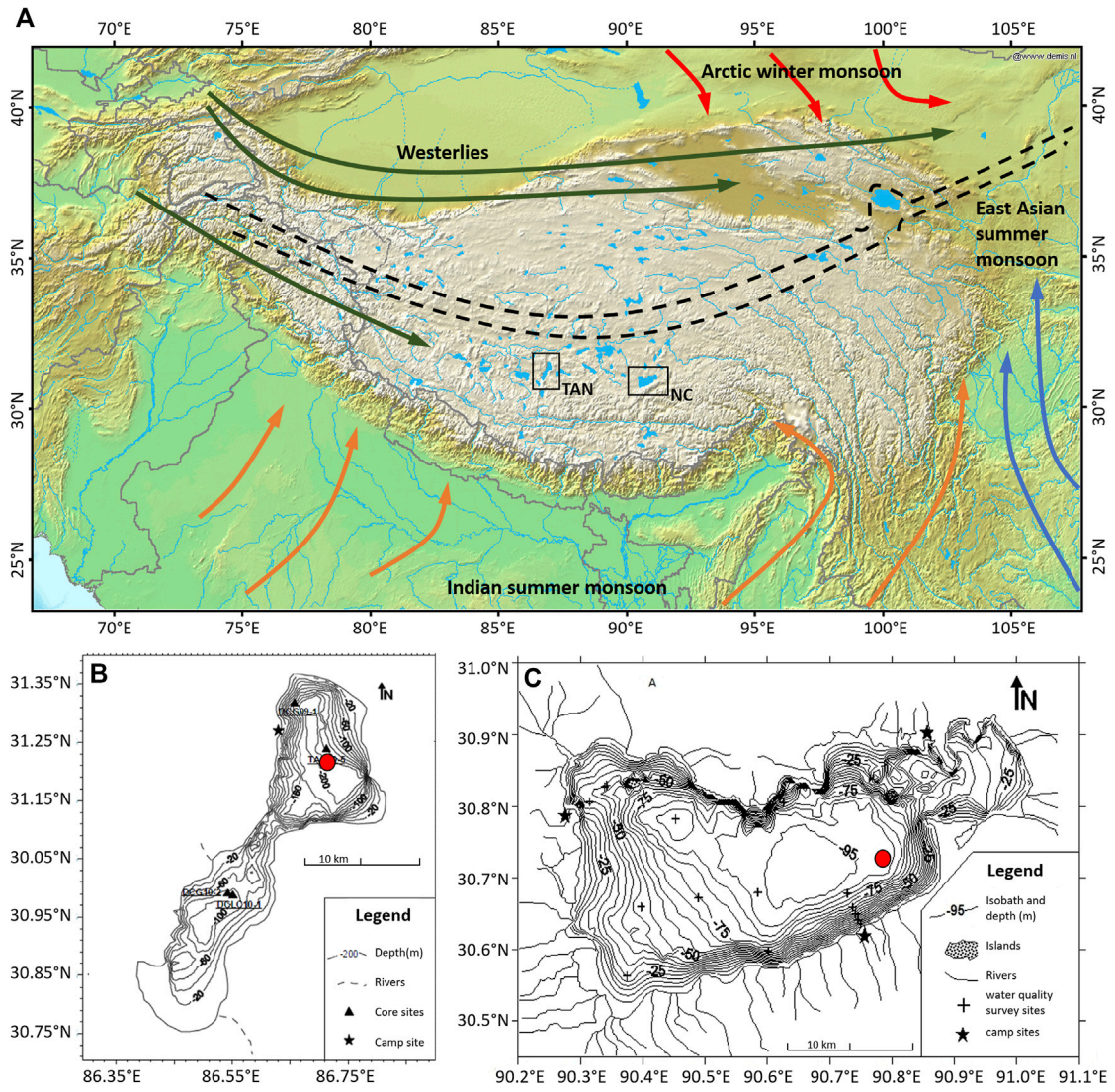

FIGURE 1
(A) Topographic map of the Tibetan Plateau showing the locations of Nam Co (NC) and Tangra Yumco (TAN) (map source: http://www.demis.nl) and the atmospheric system, including the Indian summer monsoon (ISM) in orange, the East Asian summer monsoon (EASM) in blue, and the Westerlies in green, as well as the Asian winter monsoon (AWM) in red (Anslan et al., 2020). The dotted black lines denote the summer monsoon transition zone (SMTZ) as suggested by Wünnemann et al. (2018). **(B)** Bathymetric map of Tangra Yumco with core site TAN12-2 (red dot, Wang et al., 2010), and **(C)** bathymetric map of Nam Co with core site NC08/01 (red dot, Wang et al., 2009).

2 Regional setting

The Tibetan Plateau hosts more than 300 lakes with a surface area greater than 10 km^2 (Yu et al., 2001). In our study, we investigate lacustrine records from Nam Co and Tangra Yumco, two lakes located on a west-east transect in the central and southern part of the Tibetan Plateau (Figure 1A).

Nam Co is located 230 km north of Lhasa (30°30′–30°35′ N, 90°16′–91°05′ E; Figure 1C) in an altitude of 4,718 m above sea level (a.s.l.). Nam Co is one of the largest saline lakes on the Tibetan Plateau, with a surface area of 2017 km^2 and a catchment area of 10,680 km^2 (Keil et al., 2010; Zhou et al., 2013). The maximum water depth in the central basin is 98.8 m (Wang et al., 2009; Daut et al., 2010) and it is located in a hydrologically closed basin. Lake waters are dominated by HCO_3^- and Na^+ ions, but show very low Ca^{2+} and Mg^{2+} concentrations and a Mg/Ca ratio of 17.5 mol/mol (Table 1). Carbonates precipitated in the lake are monohydrocalcite (MHC), low-Mg calcite and traces of dolomite. Extensive lake level changes are indicated by numerous lake terraces around Nam Co. The highest terrace of 140 m above present lake level was formed during the last interglacial at around 116 ka BP (Wu et al., 2004). A lacustrine terrace at 11 m above present lake level indicates the

TABLE 1 Characteristics of modern lake waters of both studied lakes Nam Co and Tangra Yumco.

Lake	Lat.	Lon.	Alt.	Water depth [m]	EC [µS/cm]	Salinity [psu]	pH	Alkalinity [mmol/L]	$\delta^{18}O$ [‰]	δD [‰]	$\delta^{13}C_{DIC}$ [‰]
Nam Co	30.67	90.81	4,725	98.8	1870	1.2	9.1	17.2	−6.1	−66.4	3.2
Tangra Yumco	31.27	86.65	4,540	230	11890	8.6	9.5	41.5	−6.5	−76.7	5.2

Lake	Ca [mg/l]	Mg [mg/l]	Fe [µg/l]	Mn [µg/l]	Ba [µg/l]	Sr [mg/l]	Mg/Ca mol	Sr/Ca mmol	Ba/Ca mmol	Fe/Ca mmol	Mn/Ca mmol
Nam Co	5.8	56.8	3.06	0.30	23.37	0.46	17.5	38.76	1.255	0.41	0.040
Tangra Yumco	22.0	278.7	61.6	1.45	5.34	0.31	22.7	6.78	0.076	2.15	0.052

Water parameters were measured on 13 September, 2011, at Tangra Yumco and on 4 July, 2018, at Nam Co.

Holocene highstand and was dated to 6 ka BP (Wallis et al., 2011) or 4.2–2.2 ka BP (Chen et al., 2017).

The present climate at Nam Co is semi-arid to sub-humid with a mean January temperature of −10.8°C and mean July temperature of 12.6°C. The lake freezes completely during the winter months with an average ice cover period of 90–130 days (Kropáček et al., 2013; Wang et al., 2019). The mean annual precipitation is 406 mm, mainly brought by the ISM from June to August (Li M. et al., 2008). The water balance is mainly controlled by precipitation, evaporation and groundwater inflow, and to a lesser extent by meltwater runoff. Zhu et al. (2010) found that precipitation on the lake and as surface runoff accounted for 63% to the water input, while glacier meltwater only contributes ~10%, and the remaining 27% are attributed to other sources, including groundwater. The P/E (precipitation/evaporation) balance is negative. More than 60 streams feed the lake, most of them discharging from the Nyainqêngtanglha mountain range in the south (Wang et al., 2009), resulting in moister conditions on the southern bank. These climatic conditions are reflected by the vegetation, which is dominated by alpine meadows and steppe grassland (e.g. *Stipa* spp., *Artemisia* spp. and *Kobresia* spp.), and is commonly used as pasture land (Miehe et al., 2008, 2009).

Tangra Yumco is located 450 km west of Lhasa and 375 km west of Nam Co (30°45′–31°22′N, 86°23′–86°49′E; Figure 1B). It is a saline closed-basin lake situated on the northern slope of the Gangdis Mountains at an altitude of 4,540 m a.s.l. The lake is situated in an active north–south trending graben system (Armijo et al., 1986) and consists of two sub-basins with a surface area of 824 km^2 and a catchment area of 8,934 km^2. The southern basin has a water depth of 100 m and the northern basin a maximum depth of 230 m, making Tangra Yumco the deepest lake on the Tibetan Plateau (Wang et al., 2010; Haberzettl et al., 2015). The modern-day water parameters of the northern basin, where the sediment core was taken, are summarized in Table 1. Tangra Yumco waters contain nearly equal amounts of HCO_3^- and SO_4^{2-} and are rich in Na^+ (>80%). High Mg/Ca molar ratios with values up to 75 were measured in Tangra Yumco in 2009 (Börner et al., 2017), but decreased to 22.7 in the following sampling years (Table 1).

The largest lake level changes observed on the Tibetan Plateau were reported for Tangra Yumco (Kong et al., 2011; Rades et al., 2015). Well-preserved paleoshorelines are located up to 185 m above the present lake level, indicating an early Holocene lake-level highstand followed by shrinkage of the large lake (Long et al., 2012; Liu et al., 2013; Rades et al., 2013). High bedrock terraces around the lake (~360 m above present lake level) reflect the mid-Pleistocene highest lake level of Tangra Yumco (Kong et al., 2011).

Tangra Yumco lies in the climatic transition between Westerly-influenced and ISM-influenced regions. Climate conditions are cold semi-arid, with a mean January temperature of −11.4°C and mean July temperature of 10.9°C (Miehe et al., 2014). During winter months, the lake is covered with ice for ~95 days but due to the high salinity it is not completely frozen in every year (Kropáček et al., 2013). Mean annual precipitation is 305 mm (Hudson and Quade, 2013) with highest rainfall during summer monsoon (Singh and Nakamura, 2009; Maussion et al., 2013; Guo et al., 2014). The water balance is predominantly controlled by precipitation and evaporation, whereas meltwater from glaciers has a minor impact and accounted for only 14% of the total basin runoff between 2001 and 2011 (Biskop et al., 2016). Two large rivers enter the currently terminal lake from the west and the southeast, discharging from the Gangdis mountain range (Long et al., 2012). Climate conditions support alpine steppe vegetation (e.g. *Stipa purpurea*, *Kobresia pygmea* and *Artemisia* spp.) used as pasture or infrequently irrigated agriculture (Miehe et al., 2014; Ma et al., 2017).

3 Material and methods

3.1 Sampling and sample preparation

Sediment core NC08/01, with a total length of 10.41 m, was recovered from 93 m water depth in the central part of Nam Co

basin (30°44.25′ N, 90°47.42′ E; Figure 1B). Gravity core NC08/01-Pilot4 (1.15 m length, 30°44.25′ N, 90°47.42′ E, 93 m water depth) forms the uppermost part of the composite profile. Sediment core TAN12-2, with a total length of 11.5 m, was retrieved from 217 m water depth in the northern basin of Tangra Yumco (31°13.93′N, 86°43.25′E; Figure 1C). Gravity core TAN10/4 (1.62 m length, 31°15.15′N, 86°43.37′E, 223 m water depth) forms the upper part of the composite profile. Piston cores were recovered using a piston coring system (Ø 90 mm; UWITEC, Mondsee, Austria) and gravity cores (Ø 63 mm) were retrieved using a modified gravity corer (Meischner and Rumohr, 1974). Details on core recovery, handling and sedimentological properties for Nam Co are given in Doberschütz et al. (2013) and Kasper et al. (2012) and for Tangra Yumco in Akita et al. (2015) and Henkel et al. (2016). For geochemical and paleontological analysis, the cores were sampled in 1 cm intervals. Bulk sediment samples for stable isotope analysis were freeze-dried and homogenized by grinding.

For paleontological analysis, sediment samples were treated with 5% hydrogen peroxide (H_2O_2) for organic matter removal, followed by washing and sieving (63 and 200 µm mesh size) with deionized water. From the 200 µm size fraction, ostracod shells were picked with a fine brush under a low magnification stereoscopic microscope. Identification was based on Hou and Gou (2002, 2007) and Wrozyna et al. (2009). For chemical analyses (REEs, trace elements and stable isotopes) only adult individuals with pristine shells from the dominant ostracod taxon *Leucocytherella sinensis* were used.

Selection of shells was done under a low magnification stereoscopic microscope by visual inspection of surface coatings or dissolution evidence. Shells were cleaned manually with a fine brush and deionized water and ethanol. After cleaning, shells were dried and split into two groups, one for stable isotope and one for REE and trace element analysis. Shells destined for stable isotope analysis were weighed (average 7 µg per shell) and 10–15 shells per sample horizon were used to reach the minimal sample weight of 80 µg. Stable isotopes of ostracod shells could not be analyzed for Tangra Yumco due to an insufficient number of available adult *L. sinensis* shells in parts of the core (Akita et al., 2015). Shells destined for REE and trace element analysis were fixed on glass slides using double-faced adhesive pads (tesa® TACK).

3.2 Analytical procedures

REE and trace element analysis was carried out using a high-resolution sector-field ICP–MS Thermo Element 2 combined with a 213 nm (UP-213) Nd:YAG laser ablation system from New Wave at the Max Planck Institute for Chemistry (MPI), Mainz (Jochum et al., 2007). Ablation was performed in a helium atmosphere and argon was the carrier gas. Line-scan analysis was performed using a 100 µm crater size with a high scan speed of 80 µm s^{-1} at an energy density of 2.6 J cm^{-2} and a repetition rate of 5 Hz. Three linescans were carried out across the surface of each single shell. For each stratigraphic horizon, two to four shells were analyzed. Isotopes measured in this study (^{25}Mg, ^{27}Al, ^{29}Si, ^{31}P, ^{43}Ca, ^{47}Ti, ^{55}Mn, ^{57}Fe, ^{63}Cu, ^{85}Rb, ^{88}Sr, ^{89}Y, ^{137}Ba, ^{139}La, ^{140}Ce, ^{141}Pr, ^{146}Nd, ^{147}Sm, ^{151}Eu, ^{157}Gd, ^{159}Tb, ^{163}Dy, ^{165}Ho, ^{167}Er, ^{169}Tm, ^{174}Yb, ^{175}Lu, ^{208}Pb, ^{232}Th, and ^{238}U) are interference-free as demonstrated by Jochum et al. (2012). NIST SRM 612 reference glass was used for external calibration. Precision of measurements ranges between 1.2 and 7.8% for all elements with increasing error at lower concentrations (i.e., 2.0% for Ba, 2.4% for Sr, 3.1% for Mg, 4.5% for U, and 7.8% for Fe). Blank-corrected count rates of the analyzed isotopes were calculated relative to the internal standard (^{43}Ca; Yang et al., 2014). Each measurement was checked for elevated Al and Ti counts to identify remaining shell contamination, such as Aluminosilicates, which would result in enhanced element counts. These sections were removed from further consideration. Elemental ratios in ostracod shells (El/Ca) are expressed in mmol/mol. REE concentrations were chondrite normalized following Haskin et al. (1968; 1971). Intra-shell and inter-shell-variability ranges from 2% (Sr), 3% (Mg, Ba), 4% (P, Mn, Y), 5% (La, Ce, Pr, Nd, Gd, Sm, Eu, and Dy), 6% (Fe, Tb, Ho, Er, Tm, Yb, and Pb), 7% (Al, Cu, Lu, and Th), 8% (Si, Ti, U), up to 9% (Rb), and lie within the analytical error margin.

Analysis of stable isotopes was done at the GFZ Potsdam, Germany. The analysis of $\delta^{18}O$ and $\delta^{13}C$ values in ostracod shells was done with a KIEL-IV-Carbonate Device connected to a Finnigan MAT253 mass spectrometer. Around 40–80 µg ostracod samples were reacted with 103% H_3PO_4 at 72°C. Standardization was done using international reference materials IAEA-NBS18 and NBS19, as well as laboratory internal standards C1 (calibrated against VPDB). The analytical precision was better than ±0.06‰ for both, $\delta^{18}O_{Lsin}$ and $\delta^{13}C_{Lsin}$ values (L_{sin} = *Leucocytherella sinensis*).

Stable isotope analysis of bulk sediment from Tangra Yumco core was carried out using a Finnigan GasBench-II with carbonate-option connected to a DELTA^{plus} XL isotope ratio mass spectrometer (IRMS). Around 200 µg of bulk sediment samples was reacted with 100% H_3PO_4 at 75°C for 60 min. Results are expressed in the standard delta notation in per mil relative to VPDB (Vienna Pee Dee Belemnite). The analytical precision was better than ±0.07‰ for $\delta^{18}O_{bulk}$ and $\delta^{13}C_{bulk}$ values.

3.3 Chronologies

AMS ^{14}C radiocarbon dating of 24 bulk sediment samples from NC08/01-Pilot4 and NC08/01 and 28 bulk sediment samples from TAN10/4 and TAN12-2 was carried out by Beta Analytics, Miami, United States A reservoir age correction of 1,420 years for Nam Co (Kasper et al., 2012; Doberschütz et al.,

2013) and 2070 years for Tangra Yumco (Haberzettl et al., 2015; Henkel et al., 2016), respectively, was applied, based on dating of surface sediments. Corrected ages were calibrated with OxCal 4.1.7 and Calib 7.0, respectively, and the age-depth model was established by applying a linear interpolation (Doberschütz et al., 2013; Haberzettl et al., 2015). The sediment records reach back to approximately 23.8 cal ka BP for Nam Co and 17.5 cal. ka BP for Tangra Yumco. The mean time resolution of intervals between bulk sediment samples is approximately 50 years, for intervals between ostracod samples approximately 100 years.

3.4 Statistics

Statistical analysis were performed on datasets comprising trace element (Mg/Ca, Sr/Ca, Ba/Ca, Mn/Ca, Fe/Ca, U/Ca), REEs (LREE = sum of light REE/Ca: La, Ce, Pr, Nd, Sm, Eu); HREE = sum of heavy REE/Ca: Gd, Tb, Dy, Ho, Er, Tm, Yb, and Lu) and stable isotope composition of ostracod shells ($\delta^{13}C_{Lsin}$, $\delta^{18}O_{Lsin}$). Dissimilarity indices, detecting underlying ecological gradients (Faith et al., 1987), were calculated for both datasets, followed by constrained hierarchical clustering to establish a hierarchical classification of the records (Grimm, 1987; Birks et al., 2012). Constrained clustering is used to detect discontinuities within the record and to identify homogeneous sections. A broken-stick model was applied to test for number of significant groups within the classification (Bennett, 1996). To allow statistical comparison between Nam Co and Tangra Yumco records all data sets were harmonized by simple linear interpolation and re-sampled in 50-years intervals. The ordination method non-metric Multidimensional Scaling (nMDS) was used on the original and harmonized datasets to explore patterns of variation within each data set. The applied distance measure was Gower. Goodness of fit is given in the stress value. We chose a 2-dimensional model, as no significant reduction in stress level was observed with increasing dimension. In order to analyze the similarity or dissimilarity between different records and to test for the significance of any relationship found, Procrustes rotation and associated PROTEST permutation test were applied to the nMDS results. Procrustes rotation finds an optimal superimposition that maximizes fit of different datasets (Gower, 1971; Peres-Neto and Jackson, 2001). The ordinations (nMDS) of both datasets are compared pair-wise and rotated or re-scaled to find the optimal fit. Procrustes rotation was performed on harmonized datasets. The effectiveness of the rotation is elevated by the residual sum-of-squares and root mean squared error (RMSE). Statistical significance is assessed by the Procrustes permutation test (PROTEST), using a correlation-like statistic derived from the symmetric Procrustes sum of squares (m_{12}) and associated *p*-value. Statistical analysis was carried out using R-software (R Core Team, 2015) and packages vegan and rioja (Juggins, 2015; Oksanen et al., 2016).

4 Results

4.1 The Nam Co ostracod shell chemistry record

Trace element ratios of ostracod shells from the whole Nam Co composite profile range from 0.39–13.21 mmol/mol for Mg/Ca, 0.6–20.3 mmol/mol for Sr/Ca, 0.04–0.38 mmol/mol for Ba, 0.09–6.47 mmol/mol for Mn/Ca, 0.04–4.82 mmol/mol for Fe/Ca, and 0.008 µmol/mol—0.6 mmol/mol for U/Ca (Figure 2). As expected, all REEs are positively correlated with each other and sum of REEs (ΣREEs) ranges from 0.006–0.22 mmol/mol. High elemental ratios are found in the lower part of the record (19–16 cal. ka BP; Figure 2), except for Sr/Ca, which is biased by aragonite precipitation, whereas the ΣREEs show lowest concentrations of the whole record. Lower El/Ca ratios are observed between 16 and 13 cal. ka BP, accompanied by a slight increase in ΣREEs from 16 to 14.5 cal. ka BP, and a peak in ΣREEs between 14.5 and 13 cal. ka BP. In addition, enrichment in light REEs is observed, as the LREE/HREE ratio increases. A strong increase in Sr/Ca and Ba/Ca ratios occurs at 13 cal. ka BP, reaching values comparable to modern ones at 12 cal. ka BP. After 10 cal. ka BP, observed elemental ratios are low and most stable. A slight increase in elemental ratios is observed at 3.8 cal ka BP accompanied by peaks in Fe/Ca and LREE/HREE. During the last 2000 years the Mg/Ca, and especially Sr/Ca and Ba/Ca ratios show again an increase, while Mn/Ca and Fe/Ca ratios and REEs remain constant. The LREE/HREE ratio decreases significantly. U/Ca values show increased variability but are decreasing since 2 cal. ka BP.

Stable isotopes in ostracod shells range between -0.04 and 2.8‰ for $\delta^{13}C_{Lsin}$ and between −8.7 and −2.1‰ for $\delta^{18}O_{Lsin}$ values (Figure 2), respectively. Both stable isotope values are high in the lowest part of the record (18–11 cal. ka BP) with a shift to more negative values at 13 cal. ka BP. After 11 cal. ka BP, $\delta^{13}C_{Lsin}$ and $\delta^{18}O_{Lsin}$ values are strongly decreasing, reaching minima around 9.5 cal ka BP. Thereafter, $\delta^{13}C_{Lsin}$ values show a gradual increase until 4 cal. ka BP, whereas $\delta^{18}O_{Lsin}$ values remain low. The last 2000 years are characterized by a rather sudden increase in both $\delta^{13}C_{Lsin}$ and $\delta^{18}O_{Lsin}$ values followed by relatively stable values.

4.2 The Tangra Yumco ostracod shell chemistry and bulk carbonate stable isotope record

In the Tangra Yumco record the ranges are 1.73–38.6 mmol/mol for Mg/Ca, 0.37–14.35 mmol/mol for Sr/Ca, 0.03–0.51 mmol/mol for Ba/Ca, 0.18–11.37 mmol/mol for Mn/Ca, 0.06–18.38 mmol/mol for Fe/Ca, and 0.06–16.93 mmol/mol for U/Ca (Figure 3). REEs are positively correlated with each other and ΣREEs ranges from −0.004–0.48 mmol/mol. In

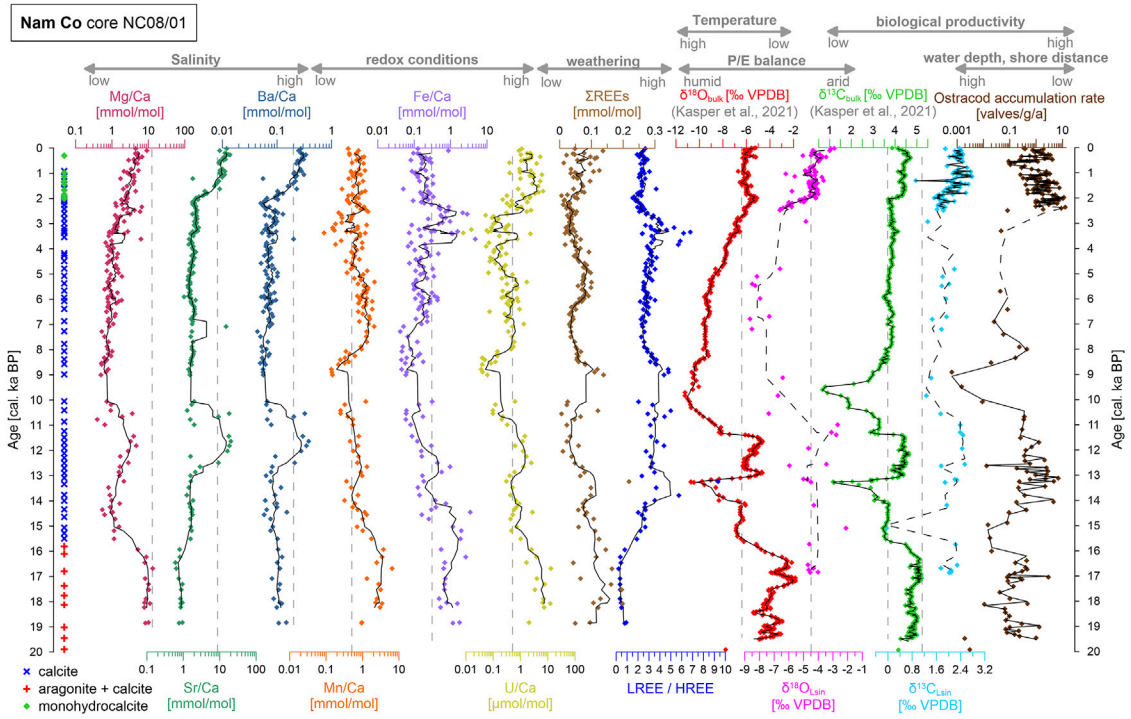

FIGURE 2
Nam Co trace element, REE and stable isotope records of ostracod shells ($\delta^{18}O_{Lsin}$ and $\delta^{13}C_{Lsin}$, Lsin = *Leucocytherella sinensis*) as well as bulk isotopes ($\delta^{18}O_{bulk}$, $\delta^{13}C_{bulk}$; Kasper et al., 2021) from core NC08/01. Authigenic carbonate mineralogy is shown on the left to indicate phases of formation of aragonite (red cross), calcite (blue x), and monohydrocalcite (green diamond). Ostracod Mg/Ca, Sr/Ca, and Ba/Ca ratios represent lake water salinity, ratios of Mn/Ca, Fe/Ca, and U/Ca reflect redox conditions and microbial activity. Rare earth elements (REEs) display weathering intensity and provenance change, where ΣREEs is the sum of light REE/Ca ratios (LREE: La, Ce, Pr, Nd, Sm, Eu) and heavy REE/Ca ratios (HREE: Gd, Tb, Dy, Ho, Er, Tm, Yb, Lu). Stable oxygen isotopes indicate changes in the precipitation to evaporation ratio (P/E) and meltwater input. Stable carbon isotopes and ostracod accumulation rate reflect biological productivity. Very low ostracod accumulation rates are indicative of oxygen deficiency, low carbonate contents or calcite dissolution. Dashed lines show levels of modern values from Börner et al. (2017). Solid black lines show 5-point smoothed data.

general, element concentrations and element variability are higher in the Tangra Yumco record than in the Nam Co record (e.g., 2.6-fold in Mg/Ca ratios), except for Sr/Ca. The lowest part of the record (17.5–16 cal. ka BP) is characterized by high elemental to calcium ratios with high variability and low ΣREEs. At 16 cal. ka BP, a major shift seems to occur as ΣREEs are increasing significantly and enrichment in LREEs is observed. Other elemental ratios seem to decrease slightly or remain stable. From 15.8 to 13.5 cal. ka BP the sedimentation rate was very low (19 cm in 2300 years; (Henkel et al., 2016). Thus, only a few ostracod samples cover this time span. Nevertheless, at 13 cal. ka BP all El/Ca ratios reach maximum concentrations and start to decrease afterwards. The highest variability in elemental ratios is observed between 13 and 10 cal. ka BP. Low El/Ca ratios are observed at 12.3 cal. ka BP, higher Sr/Ca and Ba/Ca ratios occur at 12 cal. ka BP. A second slight increase in El/Ca ratios occurs from 11 to 10 cal. ka BP. After 10 cal. ka BP, elemental ratios and LREE/HREE ratios reach lowest values, except for Mn/Ca ratios, which show still slightly increased values between 10 and 8 cal. ka BP. From 4.8 to 3.6 cal. ka BP, Mg/Ca, Ba/Ca and Mn/Ca ratios start to increase slightly, ΣREEs and U/Ca ratios reach lowest values. A shift towards very low El/Ca ratios occurs at 2.8 cal. ka BP, followed by a general, mostly distinct increase, with the uppermost sample showing highest values for all El/Ca ratios.

The isotope values of bulk sediment from TAN12-2 range between 3.3 and 7‰ for $\delta^{13}C_{bulk}$ values and −9 to 0.48‰ for $\delta^{18}O_{bulk}$ values and show a general correlation. Most positive $\delta^{13}C_{bulk}$ and $\delta^{18}O_{bulk}$ values occur before 16 cal. ka BP. Until 13 cal. ka BP, $\delta^{18}O_{bulk}$ values are stable, whereas $\delta^{13}C_{bulk}$ increases slightly until 12 cal. ka BP. Most negative values of both isotopes occur at 11.5 cal ka BP. Until 4.8 cal ka BP, $\delta^{13}C_{bulk}$ and $\delta^{18}O_{bulk}$ values increase constantly. From 4.8 to 0.8 cal ka BP, $\delta^{13}C_{bulk}$ values are constant and $\delta^{18}O_{bulk}$ values increase. The past 800 years are characterized by a decrease in $\delta^{13}C_{bulk}$ and $\delta^{18}O_{bulk}$ values.

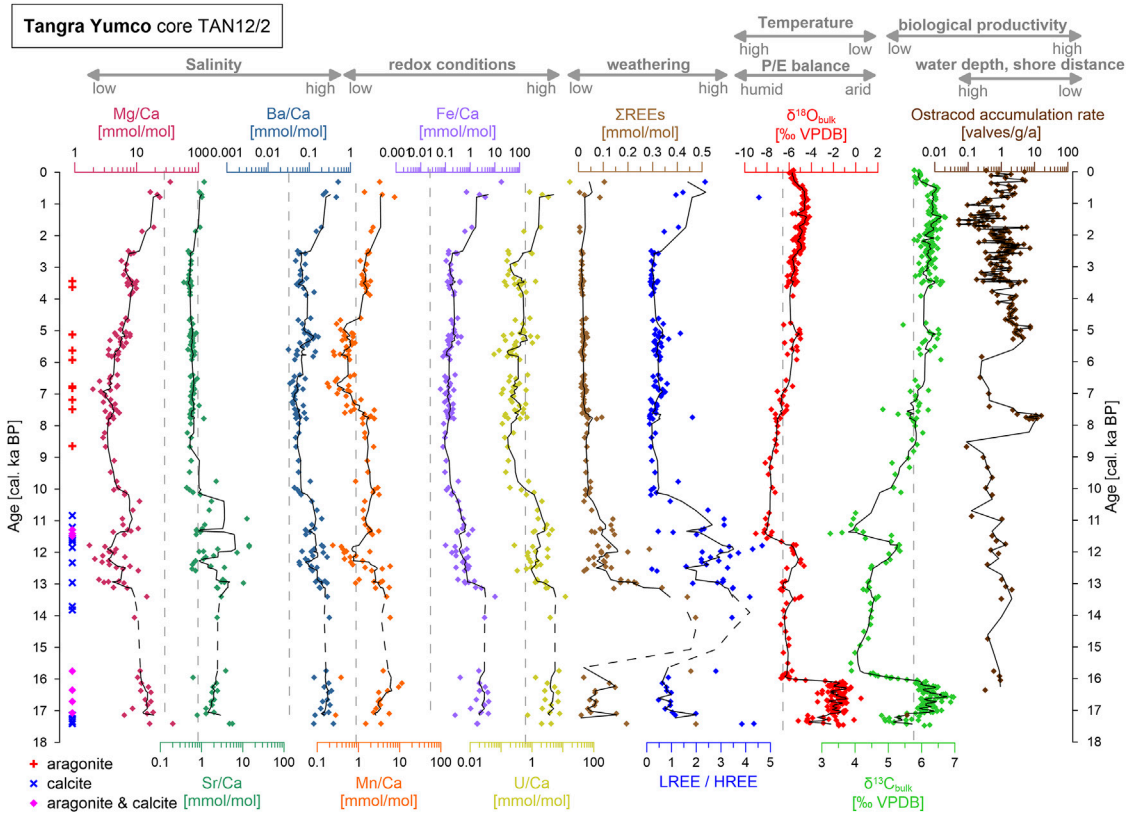

FIGURE 3
Tangra Yumco trace element and REE record of ostracod shells and stable isotopes of bulk sediment ($\delta^{18}O_{bulk}$ and $\delta^{13}C_{bulk}$) from core TAN12-2. Authigenic carbonate mineralogy is shown on the left to indicate phases of formation of aragonite (red cross), calcite (blue x), and combination of calcite and aragonite (purple diamond). Dashed lines show levels of modern values from Börner et al. (2017). Solid black lines show 5-point smoothed data. See caption of Figure 2 for more details.

4.3 Clustering and similarities of hydrological records from Nam Co and Tangra Yumco

Constrained hierarchical clustering, separating homogeneous zones, produced ten significant groups for both records, indicated by dissimilarity scores and the broken-stick model. Cluster boundaries for the Nam Co record (18.8–0 cal. ka BP) are: 15.6, 12.9, 12.2, 11.4, 8.9, 8.1, 3.6, 2, and 1 cal. ka BP. Cluster boundaries for the Tangra Yumco record (17.4–0.3 cal. ka BP) are: 17.1, 16.3, 16.1, 13.1, 11.7, 10.4, 7.7, 4.8, and 1.7 cal. ka BP. The nMDS analyses show good fit between fitted values and original distances, indicated by low stress values (Table 2). NMDS scores of original data set (Figure 4A) and harmonized data set (Figure 4B) agree very well. Procrustes rotation results, indicating the similarity and dissimilarity between records, are summarized in Table 2. Goodness of fit between datasets as well as size of residuals are illustrated in Figure 4C. Good fit is indicated by low residuals; weak fit is represented by high residuals. High residuals are observed before 15.8, from 13.4–13, 12–11.1, and at 10.5 cal. ka BP, indicating dissimilarity between both lake records. Significance of Procrustes rotation, analyzed by PROTEST, is high ($p < 0.01$, Table 2).

5 Discussion

The most important proxies including REEs and trace elements in ostracod shells, bulk isotopic data ($\delta^{18}O_{bulk}$ and $\delta^{13}C_{bulk}$), and ostracod abundance are shown versus age in Figure 2 (Nam Co) and Figure 3 (Tangra Yumco), respectively. The hydrological history of both lakes is discussed highlighting the main processes in the catchments resulting from changes in the monsoonal influence, including weathering, groundwater inflow, glacier melt, carbon burial, and important climatic periods.

5.1 Groundwater reactivation between 18.8 and 16.5 cal. ka BP

The oldest part of the Nam Co record is characterized by exceptionally low LREE/HREE ratios (Figure 2). The ΣREEs are clearly dominated by the heavy REE fraction during this period, which is four times as high as LREEs. Soils around the lake all show a LREE/HREE ratio above 1 for the present time (Li et al., 2011); transport of weathered surface material would therefore

TABLE 2 Non-metric multidimensional scaling (NMDS) stress scores, Procrustes rotation and PROTEST diagnostics to show statistical comparison between the Nam Co and Tangra Yumco records.

Data set	nMDS stress score (%)	Procrustes rotation sum of squares	RMSE	PROTEST (m_{12})	*p* value
(1) Nam Co record (original data)	12				
(2) Tangra Yumco record (original data)	7				
(3) Nam Co record (50-yr intervals)	10	4.398	0.11	0.91	0.0001
(4) Tangra Yumco record (50-yr intervals)	6				

NMDS scores are shown for the original datasets of Nam Co and Tangra Yumco (1 + 2), covering 18.9–0 cal. ka BP and 17.4–0.3 cal. ka BP, respectively, as well as for the harmonized (simple linear interpolation) data matrices in 50-years intervals (3 + 4), covering 17.4–0.3 cal. ka BP. Applied distance measure was Gower. Procrustes rotation and PROTEST were performed on harmonized datasets.

increase the LREE fraction more than the HREE fraction. Therefore, we propose that permafrost occurred in the catchment, that soils were frozen and the lake was covered by ice, which prevented any weathered material from entering the lake during this period. The source of high HREE concentrations could possibly be explained by HREEs being introduced to the lake by groundwater inflow. HREE enrichment patterns are commonly observed in groundwater, because HREEs preferably form strong dissolved complexes with organic ligands, which facilitate the transport of HREEs into solution, whereas LREEs are lost due to adsorption to Mn- and Fe-oxides (Johannesson, 2005; Och et al., 2014).

In both records, the high Mg/Ca ratios in ostracod shells as well as positive $\delta^{18}O_{bulk}$ values (Figures 2, 3) indicate high salinity and dry conditions during this period related to a shallow lake level. The very low Sr/Ca ratios are caused by aragonite precipitation in the lake, as indicated by mineralogy. Aragonite is formed under dry conditions, when lake levels decrease and salinity increases, and the Mg concentrations in lake waters reach a threshold. Aragonite is thermodynamically unstable and tends to convert to calcite, except Sr is available as it stabilizes the crystal structure (Wray and Daniels, 1957). When aragonite is formed, it removes most bio-available strontium from the water column, resulting in very low ostracod Sr/Ca ratios. The relatively low Ba/Ca ratios may also be attributed to aragonite precipitation, as Ba^{2+} adsorption is stronger in aragonite than calcite (Tunusoglu et al., 2007), but to which extent Ba incorporation into ostracod calcite is affected by aragonite is still unclear. Thus, we advise caution when interpreting the Ba/Ca signal during phases of aragonite formation. High concentrations of U/Ca and Mn/Ca ratios mirror oxygen deficiency on the lake bottom (Börner et al., 2017), which results from microbial activity decomposing organic material and from hindered CO_2 exchange with the atmosphere, which may point to prolonged ice-coverage of the lake.

In summary, Nam Co and Tangra Yumco were probably shallow lakes with suboxic conditions in the bottom water and prolonged ice coverage. These suboxic conditions could have been caused by longer ice cover and/or thermohaline stratification of the water body. These observations are supported by the highest $\delta^{18}O_{bulk}$ values (Kasper et al., 2021). Stable oxygen isotopes in closed lakes are mainly influenced by the isotopic signature of precipitation and inflowing water, which are affected by temperature and continental effects, as well as evaporative enrichment (Last and Smol, 2001). In the lake water a decrease in the P/E ratio would result in increasing $\delta^{18}O$ values as $H_2{}^{16}O$ evaporates faster than $H_2{}^{18}O$. In addition, increasing water temperatures result in decreasing $\delta^{18}O$ values of the lake water (Craig, 1965). Thus, positive $\delta^{18}O$ values reflect cold and dry conditions. Cold and arid conditions during this period were reported for many lakes on the Tibetan Plateau (Herzschuh, 2006; Günther et al., 2015), and are attributed to a weak ISM (Sirocko et al., 1993).

5.2 Increased weathering between 16.5–14 cal. ka BP

An initial increase in weathering in both records can be observed after 16.5 cal. ka BP, when the concentration in LREEs slowly starts to rise (Figures 2, 3). Increasing LREEs may be attributed to weathered material entering the lake due to a reduction in ice coverage, and the thawing of land surfaces, resulting in increased susceptibility to erosion, supporting previous findings by Kasper et al. (2015). The LREE/HREE ratio shows enrichment in LREEs, while HREE concentrations are decreasing significantly in Nam Co, suggesting increased influx of weathered material into the lake. The prominent negative shift in trace-element to calcium ratios in Nam Co sediments is indicative for decreasing salinity, reflecting an increased water supply, and permanently oxygenated conditions. The $\delta^{18}O_{bulk}$ values show a strong negative shift, indicating a decrease in salinity and thus moister conditions. Furthermore, the mineralogy changed from aragonite precipitation to calcite precipitation, which is reflected in the increasing Sr/Ca ratios. Conditions became moister due to summer monsoon strengthening and increased precipitation.

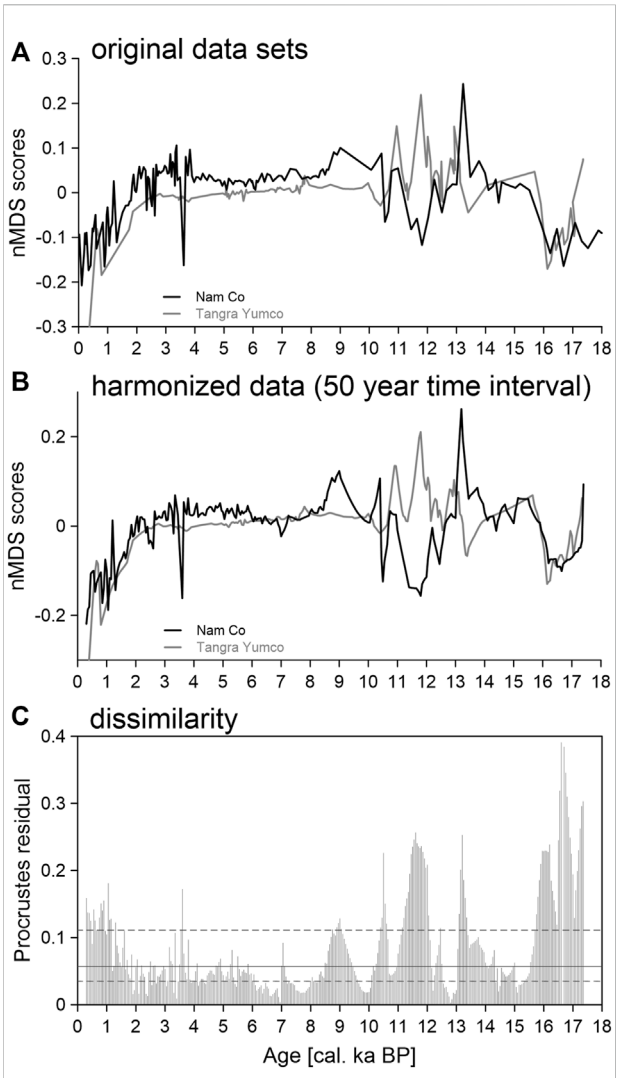

FIGURE 4
NMDS (non-metric multidimensional scaling) scores of **(A)** original and **(B)** harmonized datasets and **(C)** Procrustes rotation residuals for Nam Co and Tangra Yumco records. NMDS display patterns of variation within each record. The amplitude of Procrustes residuals reflects the degree of similarity/dissimilarity between the Nam Co and the Tangra Yumco record. Solid horizontal line shows mean deviation between records, dashed horizontal lines show the first and third quartile. Dissimilarity between both records is observed for the periods 17.4–15.8, 13.4–13, 12–11.1, 10.5, and 1.1–0.3 cal. ka BP.

In addition, glacier melt and probably permafrost thawing possibly increased the freshwater and terrigenous input.

In Tangra Yumco, the low resolution of the ostracod trace element record between 16 and 14 cal. ka BP may have missed significant change during this period, as element to calcium ratios do not show much variation. Nevertheless, an increased water input is displayed by $\delta^{18}O_{bulk}$ and $\delta^{13}C_{bulk}$ values, which both decrease rapidly. Increased moisture availability by an initial monsoonal intensification at 16 cal. ka BP was also reported by Ahlborn et al. (2016b).

5.3 Intensified glacial meltwater inflow to Nam Co between 14 and 13 cal. ka BP

The increase in REEs and the distinct positive shift in the LREE/HREE ratio during this period is caused by a significant enrichment in the LREE fraction entering the lake. Li C. et al. (2008) showed significant enrichment in LREEs over HREEs in rivers and soils around Nam Co, but the southern banks had 2- to 3-fold higher REE concentrations and LREE/HREE ratios up to 5, whereas the soils in the north show LREE/HREE ratios below 3. Accordingly, a strong increase in LREE/HREE ratios at Nam Co would suggest an increased inflow from the south, hence from the Nyainqêngtanglha mountain range, mainly caused by glacier melt. A strong freshwater pulse is also suggested by the $\delta^{13}C_{bulk}$ and $\delta^{18}O_{bulk}$ values (Kasper et al., 2021), as they display strong concomitant shifts to more negative values (Figure 2). Thus, REEs in ostracod shells enable us to assign this freshwater pulse to meltwater inflow, specifying the interpretation of the stable isotope record. Ostracod abundance increased during this period attesting better ecological conditions than before, probably higher bio-productivity caused by a warming climate.

5.4 Alternating wet and dry phases between 13 and 9 cal. ka BP

An increase in salinity after 13 cal. ka BP is reflected by increasing Mg/Ca, Sr/Ca, and Ba/Ca ratios as well as $\delta^{18}O_{Lsin}$ values (Figure 2). Salinity was higher relative to present-day values, and the lake level decreased. Redox sensitive El/Ca ratios increase during the first half of this period and $\delta^{13}C_{bulk}$ values become more positive, suggesting an increased primary productivity within the lake which resulted in oxygen depletion caused by microbial activity during decomposition of organic matter. Ice coverage of the shallow lake during the colder seasons was certainly longer than today causing restricted exchange with the atmosphere. The following decrease of Mn/Ca, Fe/Ca, and U/Ca ratios (Figure 2) was probably caused by increased oxygen supply at the lake bottom due to the low lake level allowing lake mixing to reach deeper areas. The high ostracod abundance also suggests high biological productivity as well as oxygenated conditions in a well-mixed lake. The REEs show an overall decrease, in both the light and the heavy fraction, resulting in relatively stable LREE/HREE ratios (Figure 2). The decrease in ΣREEs also supports a reduced water supply during this period. Thus, we conclude that dry conditions prevailed from 13 ka to 11.5 cal. ka BP. Our findings are supported by a strong positive shift in both $\delta^{18}O_{bulk}$ and

$\delta^{13}C_{bulk}$ values (Kasper et al., 2021), indicating generally cold and dry conditions.

After 11.5 cal. ka BP, salinity decreased again, displayed as a decrease in Mg/Ca, Sr/Ca, Ba/Ca ratios, and $\delta^{18}O_{Lsin}$ values, and total REEs rise without change in LREE/HREE ratios (Figure 2). Decreasing El/Ca ratios suggest an increase in precipitation at Nam Co, resulting in stronger weathering of soils in the whole catchment. Thus LREE/HREE ratios display no trend. This interpretation supports local inflow and erosion events as suggested by Kasper et al. (2015). Increased moisture supply is also proposed by the concomitant negative trend of δ13Cbulk and δ18Obulk values (Kasper et al., 2021), reaching lowest values at around 9.8 cal. ka BP. Ratios of U/Ca, Mn/Ca and Fe/Ca decrease further during this period and indicate a better supply of oxygen to the lake bottom.

The Tangra Yumco record shows more variability during this period, compared to the Nam Co record (Figure 3). Salinity-dependent trace elements, redox sensitive elements as well as REEs show a strong drop at the beginning of this period, indicative of increased moisture supply and rising lake levels. The increase in REE concentrations and, especially, the distinct positive peak in the light REE fraction at 11.8 cal. ka BP indicate increased weathering of the catchment. In addition, we observe an increase in $\delta^{13}C_{bulk}$ and $\delta^{18}O_{bulk}$ values, suggesting higher evaporation and a shift to drier conditions. Therefore, the increased weathering may be attributed to increased physical weathering caused by intensified winds. At 11.5 cal. ka BP, $\delta^{13}C_{bulk}$ and $\delta^{18}O_{bulk}$ values show a distinct negative shift associated with a decrease in ΣREEs and its light fraction, indicating a freshwater pulse, probably due to inflow of glacial meltwater. In addition, formation of aragonite resulted in very low Sr/Ca and Ba/Ca ratios.

5.5 Carbon burial in deep lakes during the Holocene moisture maximum between 9 and 2.6 cal. ka BP

Between 9 and 3.8 cal. ka BP salinity-indicating trace elements display low concentrations (Figures 2, 3) and thus low salinity, suggesting humid conditions and high lake levels. Variation in Mg/Ca, Ba/Ca, and Sr/Ca ratios is only minor during this period; thus, we can assume that the lake volume was sufficiently large to buffer minor climatic fluctuations. In Tangra Yumco, Sr/Ca ratios are very low (Figure 3), reflecting aragonite precipitation in the lake, which predominantly occurs under warm and wet conditions in high Mg/Ca waters. The low ostracod abundance indicates a deep profundal habitat. Productivity is high, suggested by low $\delta^{13}C_{Lsin}$ values in Nam Co (Figure 2) as well as by the higher $\delta^{13}C_{bulk}$ values in both lakes (Figures 2, 3; Kasper et al., 2021). During phases of high primary productivity ^{12}C is removed from the water, resulting in higher $\delta^{13}C_{bulk}$ values. Consequently, high amounts of organic matter accumulate on the lake bottom. The decomposition of organic matter releases preferentially ^{12}C, which can be incorporated into the ostracod calcite, resulting in a decrease in $\delta^{13}C$ values of ostracod shells (Leng and Marshall, 2004; Schwalb et al., 2013).

The significant decrease in REEs to very low values, while proportions in LREE and HREE remain constant, indicates an accumulation of organic material. In lake waters, REEs have a strong affinity to organic materials, ferromanganese oxides and carbonates, which effectively remove REEs from the water by adsorption or complexation (Johannesson and Lyons, 1994). Accordingly, very low ΣREE concentrations reflect accumulation of organic matter due to high primary productivity and an increased formation of authigenic precipitates (Johannesson, 2005; Tang and Johannesson, 2005). This interpretation is in agreement with high $\delta^{13}O_{bulk}$ and TOC values in bulk sediment, and low C/N ratios (Doberschütz et al., 2013; Kasper et al., 2021), also suggesting enhanced biogenic productivity and carbon burial.

The low U/Ca, Mn/Ca, and Fe/Ca ratios reflect well oxygenated bottom waters and low microbial activity at the beginning of this period, but increasing U/Ca and low Fe/Ca ratios after 8 cal. ka BP (Figures 2, 3) reflect the occurrence of oxygen deficiency at the lake bottom related to an increase in microbial activity. The slow but constant increase in $\delta^{18}O_{Lsin}$ values can be attributed to enhanced evaporation. The decrease in ΣREEs supports the idea of reduced inflow. This inference is supported by the slow increase in Mg/Ca ratios during the mid-Holocene indicating less moisture supply and decreasing lake levels. The slightly increasing but fluctuating Ba/Ca ratios in Tangra Yumco are likely an effect of the aragonite precipitation in the lake. However, the extent of the effect of aragonite precipitation on Ba incorporation into ostracod calcite is unknown.

5.6 Decreasing ISM intensity after 2.6 cal. ka BP

A distinct shift in moisture occurs at 2.6 cal. ka BP in Tangra Yumco and at 2 cal. ka BP in Nam Co, when trace elements in ostracods suggest increasing salinity, caused by an increase in evaporation and decrease in water supply. This increase in salinity is reflected by a strong increase in Mg/Ca, Ba/Ca (Figures 2, 3), and Sr/Ca ratios and $\delta^{18}O_{Lsin}$ values (Figure 2). However, the prominent increase in Sr/Ca and Ba/Ca ratios to values significantly higher than modern-day values, cannot be explained by evaporative enrichment alone. In Nam Co, this shift is associated with a shift in carbonate mineral formation in the lake (Kasper et al., 2013). From 2 cal. ka BP to the present, MHC is the primarily formed carbonate in Nam Co. MHC is formed in high Mg/Ca, low temperature waters under dry conditions (Han et al., 2020). The precipitation of MHC affects the chemical composition of the remaining lake water by causing enrichment

in Sr and Ba. It is still unclear to which extent MHC may affect particularly Sr and Ba in solution, and if other elements are also affected. A study by Li et al. (2012) did not find any effect of MHC precipitation on the Mg/Ca ratio of the lake water, but a significant effect on the oxygen isotopic composition. Compared to calcite, MHC seems to preferentially incorporate ^{18}O, resulting in lower $\delta^{18}O_{bulk}$ values. This carbonate ion effect on oxygen isotope ratios was also reported by Devriendt et al. (2017) for high pH and high salinity waters. This effect might explain the slight negative shift in $\delta^{18}O_{bulk}$ values (Kasper et al., 2021), which is independent from trends of other salinity proxies (Figure 2). It may reflect the combined effect of an increase in temperature, a negative P/E balance and MHC precipitation. Temperature is not captured in the ostracod trace element signatures, as temperature variations on the lake floor, especially in deep lakes, remain relatively low throughout the year.

In Nam Co, the strong initial decrease in LREE/HREE ratio shows a much stronger decrease in LREEs, compared to HREEs, suggesting continued groundwater inflow containing HREE-organic complexes (Och et al., 2014). Nevertheless, ΣREE concentrations and especially the LREE fraction show enrichment in both lakes. As salinity-indicating trace elements suggest a drier climate during this period, an increase in weathering in the catchment is unlikely. Therefore, the increase in LREEs could be associated with the reductive dissolution of Fe-Mn-oxides, on which LREEs preferentially adsorb (Och et al., 2014). This suggested process agrees with the observed increase in Mn/Ca, Fe/Ca, and U/Ca ratios, indicating amplified oxygen consumption by microbial activity, which leads to oxygen deficiency at the lake floor. Accumulation of organic matter as a result of increased lake productivity is also displayed in the high ostracod abundance. The initial increase in $\delta^{13}C_{Lsin}$ values followed by a trend to more negative values is also indicative for decomposition of organic matter, releasing ^{12}C.

A shift to wetter conditions since 300 cal. a BP is displayed in the bulk isotope data in the upper part of the Tangra Yumco record. Both isotope values show a negative trend, which can be related to an increase in precipitation intensity. This interpretation is supported by Alivernini et al. (2018) reporting a decrease in conductivity as suggested by the application of the ostracod-based conductivity transfer function. Ostracod abundance is high, indicating high primary productivity in the lake, although the so far dominant species L. sinensis disappears (Alivernini et al., 2018). As this change to moist conditions is only visible in the Tangra Yumco record, it might have been caused by an intensification in Westerly precipitation, probably because Westerlies could protrude after the ISM had retracted. Nevertheless, a lake level increase was also reported for Nam Co in recent decades, but was primarily linked to glacier melting due to the current warming (Anslan et al., 2020).

5.7 Regional synchroneity or asynchroneity of hydrological changes?

The response of lakes Nam Co and Tangra Yumco to changing climate conditions shows high similarity. Procrustes test was carried out in order to verify this visual expression and confirmed that most climatic events captured in the records occurred simultaneously. Procrustes rotation revealed a generally good fit between both records (Table 2; Figure 4). Procrustes residuals allow identification of time periods exhibiting differences in lake system response to environmental change. Highest Procrustes residuals, reflecting degree of dissimilarity between both records, occur in the periods 18–15.8, 13.4–13, and 12–11.1 cal. ka BP. During the Holocene, significant dissimilarities only occur at 10.5 cal. ka BP and after 1.1 cal ka BP. The observed dissimilarities are mainly attributed to differences in the magnitude of change. The total variation over the last 18,000 years is much higher for Tangra Yumco. For example, total variance in Mg/Ca ratios is three times higher than in Nam Co, but this may be attributed to the generally higher salinity of the lake water due to evaporative enrichment over long time scales. Additionally, the lake water volume of Nam Co is considerably higher compared to Tangra Yumco, therefore Nam Co reacts slower to climatic changes. In contrast, the observed shifts are more pronounced in the Nam Co record reacting more sensitive. Furthermore, the REE composition in both lakes is completely different during the late glacial, which also results in high Procrustes residuals. Nevertheless, both records show high similarity in amplitude and timing of hydrological changes, while during the Holocene, the changes are more gradual.

The major climatic events are best captured in the ostracods REE, Mg/Ca, Mn/Ca, and U/Ca records of both lakes and are consistent with observations from other monsoonal records (Figure 5). We identified two major phases of dry conditions at 18–16 cal. ka BP, coinciding with the "Heinrich 1 event" in the North Atlantic region (GS-2, 16.8 ka; Hemming, 2004; Figure 5), and 13–11.5 cal. ka BP, coinciding with the Younger Dryas chronozone (GS-1; Björck et al., 1998; Figure 5). Both events are also clearly displayed in records from the ISM source area Bay of Bengal (Contreras-Rosales et al., 2014), the Arabian Sea (Sirocko et al., 1993), and the East Asian monsoon (EASM) region (Wang et al., 2001; Yuan et al., 2004). The first significant transition to moist conditions is observed at 16.5 cal. ka BP in the Nam Co record. During the Greenland Interstadial 1 (GI-1) many records identified a strong increase in moisture driven by an intensification of the ISM coinciding with a phase of deglaciation (Sirocko et al., 1993; Contreras-Rosales et al., 2014). A freshwater pulse is observed after 14 ka cal. BP in the Nam Co record inferred by concomitant distinctive negative shifts in both the carbon and oxygen bulk isotopes (Kasper et al., 2021). REEs suggest that glacier melt and probably permafrost thawing increased the freshwater input during this phase. The period is less pronounced in the Tangra Yumco record due to a low sample resolution, as ostracod abundance was very low during this period. Nevertheless, many studies from the

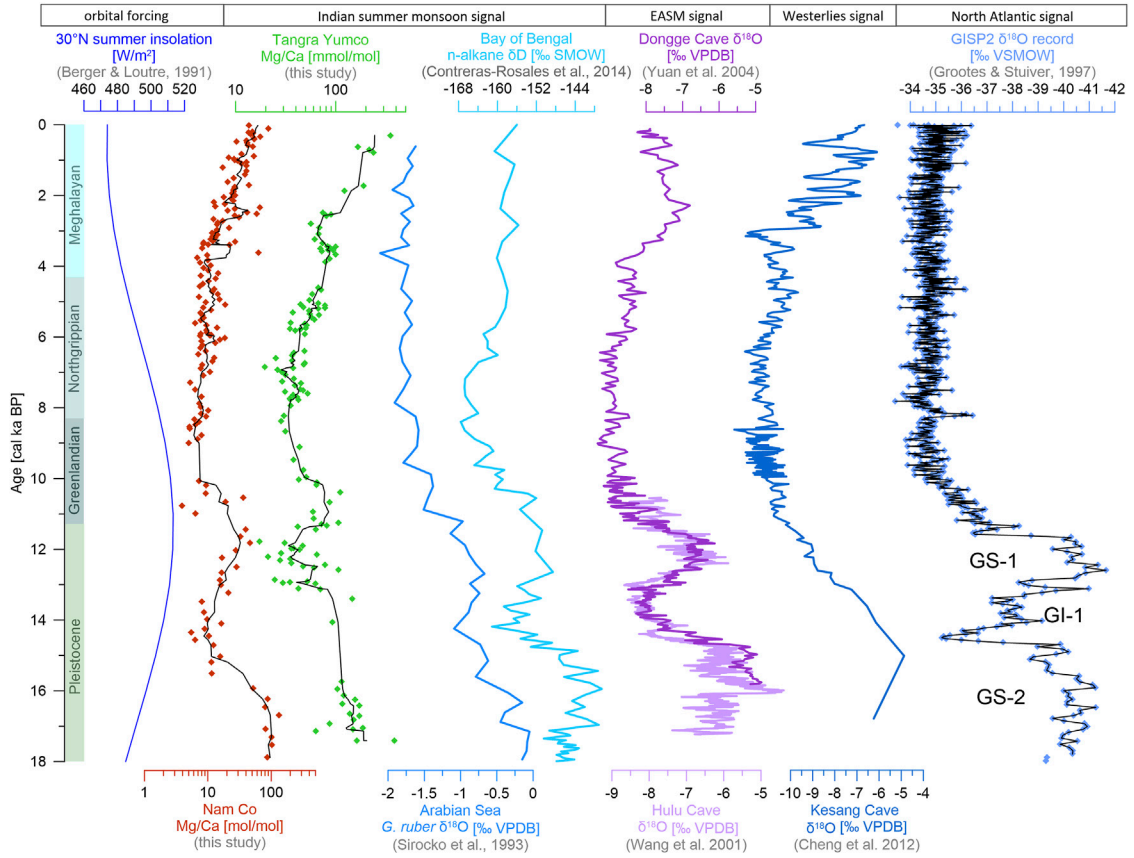

FIGURE 5
Moisture changes on the southern Tibetan Plateau based on Mg/Ca ratios of *Leucocytherella sinensis* shells from Nam Co and Tangra Yumco compared to Indian summer monsoon records from the Bay of Bengal (Contreras-Rosales et al., 2014) and Arabian Sea (Sirocko et al., 1993), East Asian monsoon records from Dongge and Hulu Cave stalagmites (Wang et al., 2001; Yuan et al., 2004), Westerlies record from Kesang Cave stalagmites (Cheng et al., 2012), as well as 30°N summer insolation showing orbital forcing (Berger and Loutre, 1991), the North Atlantic signal from the GISP2 $\delta^{18}O$ record (Grootes and Stuiver, 1997). Solid black lines show 5-point smoothed data. The GISP2 record shows major climatic events in Greenland: Greenland Stadial 2 (GS-2, "Heinrich 1 event"), Greenland Stadial 1 (GS-1, Younger Dryas chronozone) and Greenland Interstadial 1 (GI-1, Bølling/Allerød).

region inferred a first substantial increase in Asian monsoon precipitation during this period (Figure 5).

The second strengthening of the monsoon occurred at 11.5 cal. ka BP, marking the onset of the Holocene. During the early Holocene, monsoonal precipitation reached its northernmost position, and its influence was even observed in Kesang Cave on the northwestern Tibetan Plateau (Cheng et al., 2012). A strong ISM during the early to mid-Holocene (10.5–6 cal. ka BP) was reported for the Bay of Bengal and Arabian Sea (Sirocko et al., 1993; Contreras-Rosales et al., 2014) and, with some delay, at 8–4 cal. ka BP maximum monsoon strength occurred in the EASM region (Wang et al., 2001; Yuan et al., 2004). The observed strengthening in monsoonal activity at 11.5 cal ka BP, which has a pronounced effect on precipitation, coincides with the Holocene maximum solar summer insolation at 30°N (Berger and Loutre, 1991) Figure 5). Solar insolation is associated with a temperature increase and an enhanced land-sea pressure gradient, resulting in stronger monsoonal winds delivering more precipitation to the Tibetan Plateau.

The late Holocene is characterized by a decrease in water supply resulting from decreasing monsoon strength. The effect of weakening monsoon intensity during the late Holocene seems to have appeared first at Tangra Yumco and approximately 600 years later in the Nam Co area, suggesting a retreat of the ISM with an estimated velocity of approximately 600 m per year. At Tangra Yumco, there is a trend to wetter conditions and lake level increase since the Little Ice Age. This moisture increase possibly results from an intensified westerly precipitation. We hence propose a southeastward shift of the ISM-Westerly boundary since 2.6 cal. ka BP. This shift was also observed in Kesang Cave in the northwestern part of the Tibetan Plateau at 3 cal. ka BP. Cheng et al. (2012) suggested a possible shift in seasonality from wet summers to wet winters, thus indicating a weakening in ISM strength and strengthening of the Westerlies, supporting a southeastward shift of the ISM-Westerly boundary.

6 Conclusion

This study evaluated the potential of REEs as innovative ostracod shell chemistry proxies from two deep lakes to track climatic changes affecting the southern Tibetan Plateau. REEs in ostracod calcite clearly reflect weathering in the catchment. Increased total REE concentrations occur during phases of enhanced erosion due to increased precipitation intensity or strengthened winds. Furthermore, an increase in LREE/HREE ratio indicates a strong weathering effect, as LREEs are preferentially accumulated in weakly weathered soils. Based on the REE distribution in Nam Co catchment soils, an elevated input of weathered material from the southern Nyainqêngtanglha mountain range was identified, indicating increased run-off from glacier melt. High proportions of HREEs are indicative for groundwater inflow to the lake. REEs are therefore a new valuable tool to indicate changes in the sources of lake waters through time.

The well-established trace elemental ratio proxies Mg/Ca, Ba/Ca, Sr/Ca, and the $\delta^{18}O$ values are confirmed as valuable proxies for salinity, reflecting moisture availability. In addition, the asynchronous behavior of Mg/Ca, Sr/Ca, and Ba/Ca ratios are probably related to changes in carbonate minerals forming in the lake. During phases of aragonite precipitation, indicating high-Mg and high-Sr waters during dry conditions, the ostracod Sr/Ca ratios are near to zero and show no variability, whereas both Mg/Ca and Ba/Ca ratios fluctuate concomitantly but with different amplitudes. A strong increase of Sr/Ca and Ba/Ca ratios, relative to Mg/Ca ratios, reflects MHC precipitation, indicating high-Mg low-temperature waters and dry conditions. Synchronous behavior of Mg/Ca, Sr/Ca, and Ba/Ca ratios reflects calcite precipitation, thus indicating low-Mg waters and warm and moist conditions. Mn/Ca, Fe/Ca, and U/Ca ratios reflect changes in oxygen saturation based on changes in lake level and microbial activity.

Trace element and REE ratios in ostracod shells track the hydrochemical history of a lake, including oxygen supply and microbial activity in the lake, as well as weathering in the catchment. They provide high-resolution records because a single shell from one stratigraphic horizon is sufficient for analysis of trace elements and REEs, whereas stable isotope analysis requires at least 15 shells of *L. sinensis*, the most common, lightweight (~7 μg shell weight) ostracod species in lakes of the southern Tibetan Plateau. Therefore, stable isotope records often only provide low-resolution information when ostracod abundances are low.

The observed late glacial and Holocene moisture evolution is evident for many lakes on the Tibetan Plateau. On the southern Tibetan Plateau, it is mainly controlled by the interplay between the ISM and the Westerlies, representing the dominating air masses. The Last Glacial Maximum is dominated by dry and cold conditions. A significant transition to wetter conditions and rising lake levels is indicated around 16 cal. ka BP, suggesting a first strengthening of summer monsoon precipitation. The GI 1 is characterized by increased meltwater input, followed by arid conditions during the Younger Dryas. The early Holocene is marked by increasing precipitation, representing the wettest period within our records. Lake levels reached a postglacial maximum, lakes started to stratify and productivity increased. The mid and late Holocene shows a general trend of decreasing humidity. A distinct shift to dry conditions occurred 2.6 cal. ka BP in Tangra Yumco and 2 cal. ka BP in Nam Co, resulting in rapidly decreasing lake levels, caused by reduced monsoon intensity due to a southeastward migration of the ISM-Westerly boundary with an estimated velocity of approximately 600 m per year.

We conclude that the response of Nam Co and Tangra Yumco to climate change and especially monsoon intensity was in-phase during most of the late Quaternary. Moisture supply was mainly controlled by the ISM, and Westerly precipitation became more important during the past 300 years at Tangra Yumco.

Data availability statement

The datasets presented in this study can be found in online repositories. The names of the repository/repositories and accession number(s) can be found below: Pangaea database: https://doi.pangaea.de/10.1594/PANGAEA.941495.

Author contributions

NB, PF, JW, and LZ performed fieldwork and sampling. NB, MS, MA, and PF conducted ostracod identifications. NB, MS, and MA selected, cleaned and prepared ostracod shells for chemical analysis. NB, KJ, and AS performed trace element analysis, data handling, and interpretation. NB, MS, MA, BP, and AS performed stable isotope analysis and data interpretation. NB wrote the manuscript and KJ, MS, BP, AS, PF and LZ revised the manuscript.

Funding

The research presented in this manuscript was funded by the German Research Foundation (DFG) as part of the priority program 1,372 "Tibetan Plateau: Formation–Climate–Ecosystems (TiP)" (SCHW 671/14-1, FR 1473/4 and MA1308/23-2) and the National Natural Science Foundation of China (Grant 41877168). We acknowledge support by the Open Access Publication Funds of Technische Universität Braunschweig.

Acknowledgments

We thank Lailah Gifty Akita, Mauro Alivernini, and Magnus Ole Asmussen for helping to identify and pick ostracods. We are grateful to

Ulrike Weis and Brigitte Stoll (MPI for Chemistry) for laser ablation ICP-MS measurements on ostracod shells. Special thanks go to Torsten Haberzettl (University of Greifswald), Thomas Kasper (FSU Jena), and Gerhard Daut (FSU Jena) for their support during field work and retrieval of both cores. We thank Marieke Ahlborn (GFZ) and Karoline Henkel (FSU Jena) for chronological and sedimentological data. We also thank the reviewers and editor for their constructive suggestions which helped to improve this manuscript.

Conflict of interest

The authors declare that the research was conducted in the absence of any commercial or financial relationships that could be construed as a potential conflict of interest.

Publisher's Note

Supplementary material

The Supplementary Material for this article can be found online at: https://www.frontiersin.org/articles/10.3389/feart.2022.826143/full#supplementary-material

References

Ahlborn, M., Haberzettl, T., Wang, J., Fürstenberg, S., Mäusbacher, R., Mazzocco, J., et al. (2016a). Holocene lake level history of the Tangra Yumco lake system, southern-central Tibetan Plateau. *Holocene* 26, 176–187. doi:10.1177/0959683615596840

Ahlborn, M., Haberzettl, T., Wang, J., Henkel, K., Kasper, T., Daut, G., et al. (2016b). Synchronous pattern of moisture availability on the southern Tibetan plateau since 17.5 cal. Ka BP – The Tangra Yumco lake sediment record. *Boreas* 46, 229–241. doi:10.1111/bor.12204

Akita, L. G., Frenzel, P., Börner, N., Peng, P., and Wang, J. (2016). Spatial distribution and ecology of the recent ostracoda from Tangra Yumco and adjacent waters on the southern Tibetan plateau: A key to palaeoenvironmental reconstruction. *Limnologica* 59, 21–43. doi:10.1016/j.limno.2016.03.005

Akita, L. G., Frenzel, P., Haberzettl, T., Kasper, T., Wang, J., Reicherter, K., et al. (2015). Ostracoda (Crustacea) as indicators of subaqueous mass movements: An example from the large brackish lake Tangra Yumco on the southern Tibetan Plateau, China. *Palaeogeogr. Palaeoclimatol. Palaeoecol.* 419, 60–74. doi:10.1016/j.palaeo.2014.08.003

Alivernini, M., Akita, L. G., Ahlborn, M., Börner, N., Haberzettl, T., Kasper, T., et al. (2018). Ostracod-based reconstruction of Late Quaternary lake level changes within the Tangra Yumco lake system (southern Tibetan Plateau). *J. Quat. Sci.* 33, 713–720. doi:10.1002/jqs.3047

An, Z., Colman, S. M., Zhou, W., Li, X., Brown, E. T., Jull, A. J. T., et al. (2012). Interplay between the Westerlies and asian monsoon recorded in lake qinghai sediments since 32 ka. *Sci. Rep.* 2, 619. doi:10.1038/srep00619

Anslan, S., Azizi Rad, M., Buckel, J., Echeverria Galindo, P., Kai, J., Kang, W., et al. (2020). Reviews and syntheses: How do abiotic and biotic processes respond to climatic variations in the Nam Co catchment (Tibetan Plateau)? *Biogeosciences* 17, 1261–1279. doi:10.5194/bg-17-1261-2020

Armijo, R., Tapponnier, P., Mercier, J. L., and Han, T.-L. (1986). Quaternary extension in southern Tibet: Field observations and tectonic implications. *J. Geophys. Res.* 91, 13803. doi:10.1029/JB091iB14p13803

Bennett, K. D. (1996). Determination of the number of zones in a biostratigraphical sequence. *New Phytol.* 132, 155–170. doi:10.1111/j.1469-8137.1996.tb04521.x

Berger, A., and Loutre, M. F. (1991). Insolation values for the climate of the last 10 million years. *Quat. Sci. Rev.* 10, 297–317. doi:10.1016/0277-3791(91)90033-Q

Birks, H. J. B., Lotter, A. F., Juggins, S., and Smol, J. P. (2012). *Tracking environmental change using lake sediments: Volume 5. Data handling and numerical techniques*. Netherlands: Springer.

Biskop, S., Maussion, F., Krause, P., and Fink, M. (2016). Differences in the water-balance components of four lakes in the southern-central Tibetan Plateau. *Hydrol. Earth Syst. Sci.* 20, 209–225. doi:10.5194/hess-20-209-2016

Björck, S., Walker, M. J. C., Cwynar, L. C., Johnsen, S., Knudsen, K.-L., Lowe, J. J., et al. (1998). An event stratigraphy for the last termination in the north atlantic region based on the Greenland ice-core record: A proposal by the INTIMATE group. *J. Quat. Sci.* 13, 283–292. doi:10.1002/(SICI)1099-1417(199807/08)13:4<283:AID-JQS386>3.0.CO;2-A

Börner, N., De Baere, B., Akita, L. G., Francois, R., Jochum, K. P., Frenzel, P., et al. (2017). Stable isotopes and trace elements in modern ostracod shells: Implications for reconstructing past environments on the Tibetan Plateau, China. *J. Paleolimnol.* 58, 191–211. doi:10.1007/s10933-017-9971-1

Börner, N., De Baere, B., Yang, Q., Jochum, K. P., Frenzel, P., Andreae, M. O., et al. (2013). Ostracod shell chemistry as proxy for paleoenvironmental change. *Quat. Int.* 313314, 17–37. doi:10.1016/j.quaint.2013.09.041

Chen, F., Chen, J., Huang, W., Chen, S., Huang, X., Jin, L., et al. (2019). Westerlies Asia and monsoonal Asia: Spatiotemporal differences in climate change and possible mechanisms on decadal to sub-orbital timescales. *Earth. Sci. Rev.* 192, 337–354. doi:10.1016/j.earscirev.2019.03.005

Chen, F., Feng, J.-L., Hu, H.-P., Zhang, J.-F., Gao, S.-P., Liu, X.-M., et al. (2017). Potential forcing mechanisms of Holocene lake-level changes at Nam Co, Tibetan Plateau: Inferred from the stable isotopic composition of shells of the gastropod *Radix*. *Holocene* 27, 594–604. doi:10.1177/0959683616670247

Chen, F., Yu, Z., Yang, M., Ito, E., Wang, S., Madsen, D. B., et al. (2008). Holocene moisture evolution in arid central Asia and its out-of-phase relationship with Asian monsoon history. *Quat. Sci. Rev.* 27, 351–364. doi:10.1016/j.quascirev.2007.10.017

Cheng, G., and Jin, H. (2013). Permafrost and groundwater on the qinghai-tibet plateau and in northeast China. *Hydrogeol. J.* 21, 5–23. doi:10.1007/s10040-012-0927-2

Cheng, H., Zhang, P. Z., Spötl, C., Edwards, R. L., Cai, Y. J., Zhang, D. Z., et al. (2012). The climatic cyclicity in semiarid-arid central Asia over the past 500, 000 years. *Geophys. Res. Lett.* 39, L01705. doi:10.1029/2011GL050202

Contreras-Rosales, L. A., Jennerjahn, T., Tharammal, T., Meyer, V., Lückge, A., Paul, A., et al. (2014). Evolution of the Indian Summer Monsoon and terrestrial vegetation in the Bengal region during the past 18 ka. *Quat. Sci. Rev.* 102, 133–148. doi:10.1016/j.quascirev.2014.08.010

Core Team, R. (2015) R: A language and environment for statistical computing. R Foundation for Statistical ComputingURL: https://www.R-project.org. Vienna, Austria. .

Craig, H. (1965). "The measurement of oxygen isotope paleotemperatures," in *Stable isotopes in oceanographic studies and paleotemperatures*. Editor E. Tongiorgi (Pisa: Consiglio nazionale delle richerche, Laboratorio de geologia nucleare), 161–182.

Daut, G., Mäusbacher, R., Baade, J., Gleixner, G., Kroemer, E., Mügler, I., et al. (2010). Late Quaternary hydrological changes inferred from lake level fluctuations of Nam Co (Tibetan Plateau, China). *Quat. Int.* 218, 86–93. doi:10.1016/j.quaint.2010.01.001

Devriendt, L. S., McGregor, H. V., and Chivas, A. R. (2017). Ostracod calcite records the $^{18}O/^{16}O$ ratio of the bicarbonate and carbonate ions in water. *Geochim. Cosmochim. Acta* 214, 30–50. doi:10.1016/j.gca.2017.06.044

Doberschütz, S., Frenzel, P., Haberzettl, T., Kasper, T., Wang, J., Zhu, L., et al. (2013). Monsoonal forcing of Holocene paleoenvironmental change on the central Tibetan Plateau inferred using a sediment record from Lake Nam Co (Xizang, China). *J. Paleolimnol.* 51, 253–266. doi:10.1007/s10933-013-9702-1

Faith, D. P., Minchin, P. R., and Belbin, L. (1987). Compositional dissimilarity as a robust measure of ecological distance. *Vegetatio* 69, 57–68. doi:10.1007/bf00038687

Gower, J. C. (1971). "Statistical methods of comparing different multivariate analyses of the same data," in *Mathematics in the archaeological and historical sciences*. Editors F. R. Hodson, D. G. Kendall, and P. Tautu (Edinburgh: Edinburgh University Press), 138–149.

Grimm, E. C. (1987). CONISS: A fortran 77 program for stratigraphically constrained cluster analysis by the method of incremental sum of squares. *Comput. Geosci.* 13, 13–35. doi:10.1016/0098-3004(87)90022-7

Grootes, P. M., and Stuiver, M. (1997). Oxygen 18/16 variability in Greenland snow and ice with 10^{-3} to 10^{5}-year time resolution. *J. Geophys. Res.* 102, 26455–26470. doi:10.1029/97JC00880

Günther, F., Witt, R., Schouten, S., Mäusbacher, R., Daut, G., Zhu, L., et al. (2015). Quaternary ecological responses and impacts of the Indian ocean summer monsoon at Nam Co, southern Tibetan plateau. *Quat. Sci. Rev.* 112, 66–77. doi:10.1016/j.quascirev.2015.01.023

Guo, J. P., Zhai, P. M., Wu, L., Cribb, M., Li, Z. Q., Ma, Z. Y., et al. (2014). Diurnal variation and the influential factors of precipitation from surface and satellite measurements in Tibet. *Int. J. Climatol.* 34, 2940–2956. doi:10.1002/joc.3886

Haberzettl, T., Henkel, K., Kasper, T., Ahlborn, M., Su, Y., Wang, J., et al. (2015). Independently dated paleomagnetic secular variation records from the Tibetan Plateau. *Earth Planet. Sci. Lett.* 416, 98–108. doi:10.1016/j.epsl.2015.02.007

Han, L., Li, Y., Liu, X., and Yang, H. (2020). Paleoclimatic reconstruction and the response of carbonate minerals during the past 8000 years over the northeast Tibetan Plateau. *Quat. Int.* 553, 94–103. doi:10.1016/j.quaint.2020.06.009

Haskin, L. A., Helmke, P. A., Paster, T. P., and Allen, R. O. (1971). "Rare earths in meteoritic, terrestrial, and lunar matter," in *Activation analysis in geochemistry and cosmochemistry*. Editors A. Brunfelt and E. Steinnes (Oslo: Universitetsforlaget), 202–218.

Haskin, L. A., Wildeman, T. R., and Haskin, M. A. (1968). An accurate procedure for the determination of the rare earths by neutron activation. *J. Radioanal. Chem.* 1, 337–348. doi:10.1007/bf02513689

He, Y., Hou, J., Brown, E. T., Xie, S., and Bao, Z. (2018). Timing of the Indian summer monsoon onset during the early Holocene: Evidence from a sediment core at linggo Co, central Tibetan plateau. *Holocene* 28, 755–766. doi:10.1177/0959683617744267

Hemming, S. R. (2004). Heinrich events: Massive late Pleistocene detritus layers of the North Atlantic and their global climate imprint. *Rev. Geophys.* 42, RG1005. doi:10.1029/2003rg000128

Henkel, K., Haberzettl, T., St-Onge, G., Wang, J., Ahlborn, M., Daut, G., et al. (2016). High-resolution paleomagnetic and sedimentological investigations on the Tibetan plateau for the past 16 ka cal B.P.—the Tangra Yumco record. *Geochem. Geophys. Geosyst.* 17, 774–790. doi:10.1002/2015gc006023

Herzschuh, U. (2006). Palaeo-moisture evolution in monsoonal Central Asia during the last 50, 000 years. *Quat. Sci. Rev.* 25, 163–178. doi:10.1016/j.quascirev.2005.02.006

Holmes, J. A. (1996). Trace-element and stable-isotope geochemistry of non-marine ostracod shells in Quaternary palaeoenvironmental reconstruction. *J. Paleolimnol.* 15, 223–235. doi:10.1007/bf00213042

Holmes, J. A., Zhang, J., Chen, F., and Qiang, M. (2007). Paleoclimatic implications of an 850-year oxygen-isotope record from the northern Tibetan Plateau. *Geophys. Res. Lett.* 34, L23403. doi:10.1029/2007gl032228

Holmes, J., and De Deckker, P. (2012). "The chemical composition of ostracod shells: Applications in quaternary palaeoclimatology," in *Ostracoda as proxies for quaternary climate change*. Editors D. Horne, J. Holmes, F. Viehberg, and J. Rodriguez-Lazaro (Oxford, UK: Elsevier Science), 131–143.

Hou, Y., and Gou, Y. (2002). *Fossil ostracoda of China, volume 1: Superfamilies cypridacea and darwinulidacea*. China: Science Press.

Hou, Y., and Gou, Y. (2007). *Fossil ostracoda of China, volume 2: Cytheracea and cytherellidae*. China: Science Press.

Huang, B., Yang, L., and Fan, Y. (1985). Ostracodes from surface deposits of recent lakes in Xizang. *Acta micropalaeont. Sin.* 2, 369–376. (in Chinese).

Hudson, A. M., and Quade, J. (2013). Long-term east-west asymmetry in monsoon rainfall on the Tibetan Plateau. *Geology* 41, 351–354. doi:10.1130/g33837.1

Jochum, K. P., Scholz, D., Stoll, B., Weis, U., Wilson, S. A., Yang, Q., et al. (2012). Accurate trace element analysis of speleothems and biogenic calcium carbonates by LA-ICP-MS. *Chem. Geol.* 318-319, 31–44. doi:10.1016/j.chemgeo.2012.05.009

Jochum, K. P., Stoll, B., Herwig, K., and Willbold, M. (2007). Validation of LA-ICP-MS trace element analysis of geological glasses using a new solid-state 193 nm Nd: YAG laser and matrix-matched calibration. *J. Anal. At. Spectrom.* 22, 112–121. doi:10.1039/b609547j

Johannesson, K. H., and Lyons, W. B. (1994). The rare Earth element geochemistry of Mono Lake water and the importance of carbonate complexing. *Limnol. Oceanogr.* 39, 1141–1154. doi:10.4319/lo.1994.39.5.1141

Johannesson, K. H. (2005). *Rare earth elements in groundwater flow systems*. Netherlands: Springer.

Juggins, S. (2015). rioja: Analysis of quaternary science data. R package version (0.9-5), (). http://cran.r-project.org/package=rioja.

Kasper, T., Frenzel, P., Haberzettl, T., Schwarz, A., Daut, G., Meschner, S., et al. (2013). Interplay between redox conditions and hydrological changes in sediments from Lake Nam Co (Tibetan Plateau) during the past 4000cal BP inferred from geochemical and micropaleontological analyses. *Palaeogeogr. Palaeoclimatol. Palaeoecol.* 392, 261–271. doi:10.1016/j.palaeo.2013.09.027

Kasper, T., Haberzettl, T., Doberschütz, S., Daut, G., Wang, J., Zhu, L., et al. (2012). Indian ocean summer monsoon (IOSM)-dynamics within the past 4 ka recorded in the sediments of lake Nam Co, central Tibetan plateau (China). *Quat. Sci. Rev.* 39, 73–85. doi:10.1016/j.quascirev.2012.02.011

Kasper, T., Haberzettl, T., Wang, J., Daut, G., Doberschütz, S., Zhu, L., et al. (2015). Hydrological variations on the Central Tibetan Plateau since the Last Glacial Maximum and their teleconnection to inter-regional and hemispheric climate variations. *J. Quat. Sci.* 30, 70–78. doi:10.1002/jqs.2759

Kasper, T., Wang, J., Schwalb, A., Daut, G., Plessen, B., Zhu, L., et al. (2021). Precipitation dynamics on the Tibetan Plateau during the Late Quaternary – hydroclimatic sedimentary proxies versus lake level variability. *Glob. Planet. Change* 205, 103594. doi:10.1016/j.gloplacha.2021.103594

Keil, A., Berking, J., Mügler, I., Schütt, B., Schwalb, A., Steeb, P., et al. (2010). Hydrological and geomorphological basin and catchment characteristics of lake Nam Co, south-central tibet. *Quat. Int.* 218, 118–130. doi:10.1016/j.quaint.2009.02.022

Kong, P., Na, C., Brown, R. J., Fabel, D., Freeman, S., Xiao, W., et al. (2011). Cosmogenic ^{10}Be and ^{26}Al dating of paleolake shorelines in Tibet. *J. Asian Earth Sci.* 41, 263–273. doi:10.1016/j.jseaes.2011.02.016

Kropáček, J., Maussion, F., Chen, F., Hoerz, S., and Hochschild, V. (2013). Analysis of ice phenology of lakes on the Tibetan Plateau from MODIS data. *Cryosphere* 7, 287–301. doi:10.5194/tc-7-287-2013

W. M. Last and J. P. Smol (Editors) (2001). *Tracking environmental change using lake sediments: Volume 2: Physical and geochemical methods* (Netherlands: Springer).

Leng, M. J., and Marshall, J. D. (2004). Palaeoclimate interpretation of stable isotope data from lake sediment archives. *Quat. Sci. Rev.* 23, 811–831. doi:10.1016/j.quascirev.2003.06.012

Li, C., Kang, S., Wang, X., Ajmone-Marsan, F., and Zhang, Q. (2008a). Heavy metals and rare Earth elements (REEs) in soil from the Nam Co Basin, Tibetan Plateau. *Environ. Geol.* 53, 1433–1440. doi:10.1007/s00254-007-0752-4

Li, M., Kang, S., Zhu, L., You, Q., Zhang, Q., Wang, J., et al. (2008b). Mineralogy and geochemistry of the Holocene lacustrine sediments in Nam Co, tibet. *Quat. Int.* 187, 105–116. doi:10.1016/j.quaint.2007.12.008

Li, M., Wang, J., Zhu, L., Wang, L., and Yi, C. (2012). Distribution and formation of monohydrocalcite from surface sediments in Nam Co Lake, Tibet. *Quat. Int.* 263, 85–92. doi:10.1016/j.quaint.2012.01.035

Li, M., Zhu, L., Wang, J., Wang, L., Yi, C., Galy, A., et al. (2011). Multiple implications of rare Earth elements for Holocene environmental changes in Nam Co, Tibet. *Quat. Int.* 236, 96–106. doi:10.1016/j.quaint.2010.12.022

Li, Y., Zhu, L., and Li, B. (2002). Environmental changes and Ostracoda in the Chen Co lake of southern 700 Tibet in recent 1400 years. *Acta Geogr. Sin.* 57, 413–421.

Lin, Q., Xu, L., Hou, J., Liu, Z., Jeppesen, E., Han, B.-P., et al. (2017). Responses of trophic structure and zooplankton community to salinity and temperature in Tibetan lakes: Implication for the effect of climate warming. *Water Res.* 124, 618–629. doi:10.1016/j.watres.2017.07.078

Liu, X., Lai, Z., Zeng, F., Madsen, D. B., and E, C. (20132016). Holocene lake level variations on the Qinghai-Tibetan Plateau. *Int. J. Earth Sci.* 102, 2007. doi:10.1007/s00531-013-0896-2

Long, H., Lai, Z., Frenzel, P., Fuchs, M., and Haberzettl, T. (2012). Holocene moist period recorded by the chronostratigraphy of a lake sedimentary sequence from Lake Tangra Yumco on the south Tibetan Plateau. *Quat. Geochronol.* 10, 136–142. doi:10.1016/j.quageo.2011.11.005

Ma, Q., Zhu, L., Wang, J., Ju, J., Lü, X., Wang, Y., et al. (2017). Artemisia/Chenopodiaceae ratio from surface lake sediments on the central and Western Tibetan Plateau and its application. *Palaeogeogr. Palaeoclimatol. Palaeoecol.* 479, 138–145. doi:10.1016/j.palaeo.2017.05.002

Maussion, F., Scherer, D., Mölg, T., Collier, E., Curio, J., Finkelnburg, R., et al. (2013). Precipitation seasonality and variability over the Tibetan Plateau as resolved by the High Asia reanalysis. *J. Clim.* 27, 1910–1927. doi:10.1175/jcli-d-13-00282.1

Meischner, D., and Rumohr, J. (1974). A light-weight, high-momentum gravity corer for subaqueous sediments. *Senckenberg. Maritima* 6, 105–117.

Miehe, G., Miehe, S., Kaiser, K., Reudenbach, C., Behrendes, L., La, D., et al. (2009). How old is pastoralism in tibet? An ecological approach to the making of a Tibetan landscape. *Palaeogeogr. Palaeoclimatol. Palaeoecol.* 276, 130–147. doi:10.1016/j.palaeo.2009.03.005

Miehe, G., Miehe, S., Will, M., Opgenoorth, L., Duo, L., Dorgeh, T., et al. (2008). An inventory of forest relicts in the pastures of Southern Tibet (Xizang A.R., China). *Plant Ecol.* 194, 157–177. doi:10.1007/s11258-007-9282-0

Miehe, S., Miehe, G., van Leeuwen, J. N., Wrozyna, C., van der Knaap, W., Duo, L., et al. (2014). Persistence of Artemisia steppe in the Tangra Yumco basin, west-central tibet, China: Despite or in consequence of Holocene lake-level changes? *J. Paleolimnol.* 51, 267–285. doi:10.1007/s10933-013-9720-z

Mischke, S., Aichner, B., Diekmann, B., Herzschuh, U., Plessen, B., Wünnemann, B., et al. (2010). Ostracods and stable isotopes of a late glacial and Holocene lake record from the NE Tibetan Plateau. *Chem. Geol.* 276, 95–103. doi:10.1016/j.chemgeo.2010.06.003

Mischke, S., Kramer, M., Zhang, C., Shang, H., Herzschuh, U., Erzinger, J., et al. (2008). Reduced early Holocene moisture availability in the Bayan Har Mountains, northeastern Tibetan Plateau, inferred from a multi-proxy lake record. *Palaeogeogr. Palaeoclimatol. Palaeoecol.* 267, 59–76. doi:10.1016/j.palaeo.2008.06.002

Mischke, S. (2012). Quaternary ostracods from the Tibetan Plateau and their significance for environmental and climate-change studies. *Dev. Quatern. Sci.* 17, 263–279.

Och, L. M., Müller, B., Wichser, A., Ulrich, A., Vologina, E. G., Sturm, M., et al. (2014). Rare Earth elements in the sediments of lake baikal. *Chem. Geol.* 376, 61–75. doi:10.1016/j.chemgeo.2014.03.018

Oksanen, J., Blanchet, F. G., Kindt, R., Legendre, P., Minchin, P. R., O'Hara, R. B., et al. (2016). vegan: Community ecology package. R package version 2.3-4 (). https://CRAN.R-project.org/package=vegan.

Peng, P., Zhu, L., Frenzel, P., Wrozyna, C., and Ju, J. (2013). Water depth related ostracod distribution in Lake Pumoyum Co, southern Tibetan Plateau. *Quat. Int.* 313–314, 47–55. doi:10.1016/j.quaint.2013.08.054

Peres-Neto, P. R., and Jackson, D. A. (2001). How well do multivariate data sets match? The advantages of a procrustean superimposition approach over the mantel test. *Oecologia* 129, 169–178. doi:10.1007/s004420100720

Rades, E. F., Hetzel, R., Xu, Q., and Ding, L. (2013). Constraining Holocene lake-level highstands on the Tibetan plateau by ^{10}Be exposure dating: A case study at Tangra Yumco, southern tibet. *Quat. Sci. Rev.* 82, 68–77. doi:10.1016/j.quascirev.2013.09.016

Rades, E. F., Tsukamoto, S., Frechen, M., Xu, Q., and Ding, L. (2015). A lake-level chronology based on feldspar luminescence dating of beach ridges at Tangra Yum Co (southern Tibet). *Quat. Res.* 83, 469–478. doi:10.1016/j.yqres.2015.03.002

Schwalb, A., Dean, W. E., Güde, H., Hanisch, S., Sobek, S., Wessels, M., et al. (2013). Benthic ostracode δ^{13}C as sensor for early Holocene establishment of modern circulation patterns in Central Europe. *Quat. Sci. Rev.* 66, 112–122. doi:10.1016/j.quascirev.2012.10.032

Singh, P., and Nakamura, K. (2009). Diurnal variation in summer precipitation over the central Tibetan Plateau. *J. Geophys. Res.* 114, D20107. doi:10.1029/2009jd011788

Sirocko, F., Sarnthein, M., Erlenkeuser, H., Lange, H., Arnold, M., Duplessy, J. C., et al. (1993). Century-scale events in monsoonal climate over the past 24, 000 years. *Nature* 364, 322–324. doi:10.1038/364322a0

Tang, J., and Johannesson, K. H. (2005). Adsorption of rare Earth elements onto Carrizo sand: Experimental investigations and modeling with surface complexation. *Geochim. Cosmochim. Acta* 69, 5247–5261. doi:10.1016/j.gca.2005.06.021

Thompson, L. G., Yao, T., Davis, M. E., Mosley-Thompson, E., Wu, G., Porter, S. E., et al. (2018). Ice core records of climate variability on the Third Pole with emphasis on the Guliya ice cap, Western Kunlun Mountains. *Quat. Sci. Rev.* 188, 1–14. doi:10.1016/j.quascirev.2018.03.003

Tunusoglu, Ouml, Shahwan, T., and Eroglu, A. E. (2007). Retention of aqueous Ba^{2+} ions by calcite and aragonite over a wide range of concentrations: Characterization of the uptake capacity, and kinetics of sorption and precipitate formation. *Geochem. J.* 41, 379–389. doi:10.2343/geochemj.41.379

Wallis, S. R., Nakamura, T., Mori, H., Ozawa, K., Mitsuishi, M., Shirakawa, C., et al. (2011). ^{14}C dating of Tufa deposits around lake Nam Co, Tibet. *Summaries of Researches at Nagoya University Using AMS*, 22, 174–179.

Wang, J., Huang, L., Ju, J., Daut, G., Wang, Y., Ma, Q., et al. (2019). Spatial and temporal variations in water temperature in a high-altitude deep dimictic mountain lake (Nam Co), central Tibetan Plateau. *J. Gt. Lakes. Res.* 45, 212–223. doi:10.1016/j.jglr.2018.12.005

Wang, J., Peng, P., Ma, Q., and Zhu, L. (2010). Modern limnological features of Tangra Yumco and Zhari Namco, Tibetan Plateau. *J. Lake Sci.* 22, 629–632. (in chinese with english abstract).

Wang, J., Zhu, L., Daut, G., Ju, J., Lin, X., Wang, Y., et al. (2009). Investigation of bathymetry and water quality of Lake Nam Co, the largest lake on the central Tibetan Plateau, China. *Limnology* 10, 149–158. doi:10.1007/s10201-009-0266-8

Wang, Y. J., Cheng, H., Edwards, R. L., An, Z. S., Wu, J. Y., Shen, C. C., et al. (2001). A high-resolution absolute-dated late Pleistocene Monsoon record from Hulu Cave, China. *Science* 294, 2345–2348. doi:10.1126/science.1064618

Wray, J. L., and Daniels, F. (1957). Precipitation of calcite and aragonite. *J. Am. Chem. Soc.* 79, 2031–2034. doi:10.1021/ja01566a001

Wrozyna, C., Frenzel, P., Xie, M., Zhu, L., and Schwalb, A. (2009). A taxonomical and ecological overview of Recent and Holocene ostracodes of the Nam Co region, southern Tibet. *Quat. Sci. (China)* 29, 665–677. doi:10.3969/j.issn.1001-7410.2009.04.02

Wu, Z., Zhao, X., Wu, Z., Zhou, C., Yan, F., Mai, X., et al. (2004). Palaeovegetation, palaeoclimate and lake-level change since 120 ka BP in Nam Co, central Xizang. *Acta Geol. Sin.* 78, 242–252. (in chinese with english abstract).

Wünnemann, B., Yan, D., Andersen, N., Riedel, F., Zhang, Y., Sun, Q., et al. (2018). A 14 ka high-resolution δ^{18}O lake record reveals a paradigm shift for the process-based reconstruction of hydroclimate on the northern Tibetan Plateau. *Quat. Sci. Rev.* 200, 65–84. doi:10.1016/j.quascirev.2018.09.040

Yang, Q., Jochum, K. P., Stoll, B., Weis, U., Börner, N., Schwalb, A., et al. (2014). Trace element variability in single ostracod valves as a proxy for hydrochemical change in Nam Co, central Tibet, during the Holocene. *Palaeogeogr. Palaeoclimatol. Palaeoecol.* 399, 225–235. doi:10.1016/j.palaeo.2014.01.014

Yao, T., Thompson, L., Yang, W., Yu, W., Gao, Y., Guo, X., et al. (2012). Different glacier status with atmospheric circulations in Tibetan Plateau and surroundings. *Nat. Clim. Change* 2, 663–667. doi:10.1038/nclimate1580

Ye, D.-Z., and Wu, G.-X. (1998). The role of the heat source of the Tibetan Plateau in the general circulation. *Meteorl. Atmos. Phys.* 67, 181–198. doi:10.1007/bf01277509

Yu, G., Harrison, S. P., and Xue, B. (2001). *Lake status records from China: Data base documentation*. Jena, Germany: Max-Planck-Institute fur Biogeochemie.

Yuan, D., Cheng, H., Edwards, R. L., Dykoski, C. A., Kelly, M. J., Zhang, M., et al. (2004). Timing, duration, and transitions of the last interglacial Asian monsoon. *Sci. (New York, N.Y.)* 304, 575–578. doi:10.1126/science.1091220

Zhang, J., Holmes, J. A., Chen, F., Qiang, M., Zhou, A., Chen, S., et al. (2009). An 850-year ostracod-shell trace-element record from Sugan Lake, northern Tibetan Plateau, China: Implications for interpreting the shell chemistry in high-Mg/Ca waters. *Quat. Int.* 194, 119–133. doi:10.1016/j.quaint.2008.05.003

Zhou, S., Kang, S., Chen, F., and Joswiak, D. R. (2013). Water balance observations reveal significant subsurface water seepage from Lake Nam Co, south-central Tibetan Plateau. *J. Hydrol. X.* 491, 89–99. doi:10.1016/j.jhydrol.2013.03.030

Zhu, L., Wu, Y., Wang, J., Lin, X., Ju, J., Xie, M., et al. (2008). Environmental changes since 8.4 ka reflected in the lacustrine core sediments from Nam Co, central Tibetan Plateau, China. *Holocene* 18, 831–839. doi:10.1177/0959683608091801

Zhu, L., Xie, M., and Wu, Y. (2010). Quantitative analysis of lake area variations and the influence factors from 1971 to 2004 in the Nam Co basin of the Tibetan Plateau. *Chin. Sci. Bull.* 55, 1294–1303. doi:10.1007/s11434-010-0015-8

Zhu, L., Zhen, X., Wang, J., Lü, H., Xie, M., Kitagawa, H., et al. (2009). A ~30, 000-year record of environmental changes inferred from Lake Chen Co, Southern Tibet. *J. Paleolimnol.* 42, 343–358. doi:10.1007/s10933-008-9280-9